NASA TECHNICAL NOTE

NASA TN D-6748

FLIGHT-TEST RESULTS FROM TWO TOTAL TEMPERATURE PROBES FOR AIR-DATA MEASUREMENTS UP TO 2014° K (3625° R)

by Jack Nugent, Glenn M. Sakamoto, and Lannie D. Webb

Flight Research Center
Edwards, Calif. 93523

NATIONAL AERONAUTICS AND SPACE ADMINISTRATION • WASHINGTON, D. C. • MARCH 1972

1. Report No.	2. Government Accession No.	3. Recipient's Catalog No.
NASA TN D-6748		

4. Title and Subtitle	5. Report Date
FLIGHT-TEST RESULTS FROM TWO TOTAL TEMPERATURE PROBES FOR AIR-DATA MEASUREMENTS UP TO 2014° K (3625° R)	March 1972
	6. Performing Organization Code

7. Author(s)	8. Performing Organization Report No.
Jack Nugent, Glenn M. Sakamoto, and Lannie D. Webb	H-668
	10. Work Unit No.
	126-61-16-00-24

9. Performing Organization Name and Address	11. Contract or Grant No.
NASA Flight Research Center P. O. Box 273 Edwards, California 93523	
	13. Type of Report and Period Covered
12. Sponsoring Agency Name and Address	Technical Note
National Aeronautics and Space Administration Washington, D. C. 20546	14. Sponsoring Agency Code

15. Supplementary Notes

16. Abstract

An experimental temperature probe package containing a fluidic oscillator temperature probe and a shielded thermocouple temperature probe was tested during several X-15 flights. The X-15 flights provided greatly varying test conditions, including a wide range of rapidly changing total temperatures and Mach numbers which extended from subsonic to hypersonic speeds.

Within restricted ranges of free-stream Mach number, free-stream unit weight flow, and local stagnation pressure, both probes yielded ramp outputs of temperature parallel to ramp inputs of free-stream total temperature. Within these ranges both probes were used to determine total temperature in the Mach 6 temperature environment. Because ambient temperature was known, both probes were used to estimate velocity and Mach number.

The differences between total temperature, velocity, and Mach number obtained from the fluidic oscillator probe and corresponding free-stream values increased with increasing free-stream total temperatures and decreased with increasing free-stream unit weight flow.

Temperature, velocity, and Mach number obtained from the shielded thermocouple probe essentially agreed with corresponding free-stream values.

17. Key Words (Suggested by Author(s))	18. Distribution Statement
Temperature probes Hypersonic flight Air-data parameters	Unclassified - Unlimited

19. Security Classif. (of this report)	20. Security Classif. (of this page)	21. No. of Pages	22. Price*
Unclassified	Unclassified	51	$3.00

*For sale by the National Technical Information Service, Springfield, Virginia 22151

FLIGHT-TEST RESULTS FROM TWO TOTAL TEMPERATURE PROBES FOR AIR-DATA MEASUREMENTS UP TO 2014° K (3625° R)

Jack Nugent, Glenn M. Sakamoto, and Lannie D. Webb
Flight Research Center

INTRODUCTION

Measuring air-data parameters is one of the difficult tasks associated with flight-test programs on research aircraft. Flight measurements of velocity, Mach number, total temperature, and other parameters are needed to plan and conduct research flights as well as to evaluate research findings. In the X-15 program, a combination of data from onboard sensors, ground-based radar, and meteorological soundings was used to obtain the needed air-data parameters (ref. 1). One of the onboard sensors which proved to be particularly useful was a shielded thermocouple probe which measured free-stream total temperature.

Interest in techniques of measuring free-stream total temperature beyond the present capability of thermocouple probes led the NASA Flight Research Center to install a piggyback temperature probe package on the X-15 airplane for several flights. The experimental package contained a fluidic oscillator temperature probe and the previously tested shielded thermocouple probe (ref. 2). These probes were exposed to the large range of total temperature and the accompanying variations of airplane Mach number, altitude, and angle of attack which occur over a flight range extending from subsonic to hypersonic speeds.

This report presents and analyzes data from the fluidic oscillator temperature probe and the shielded thermocouple temperature probe from four X-15 flights. Total temperature ranged from approximately 244° K (439° R) to approximately 2014° K (3625° R), with an accompanying Mach number range from approximately 0.8 to approximately 6.7. The altitude range extended from approximately 13,700 meters (45,000 feet) to approximately 81,500 meters (267,500 feet), although probe data were not obtained over this entire range. Data were obtained under rapidly changing flow conditions because of the rapid accelerations and decelerations encountered in the X-15 flight.

In the analysis, the total temperature measurement from each probe was compared with free-stream total temperature. Free-stream total temperature was calculated from free-stream velocity and ambient temperature, obtained from ground-based radar and meteorological soundings. In addition, velocities and Mach numbers derived from probe temperatures and ambient temperatures were compared with free-stream values. Differences between total temperature, velocity, and Mach number derived from each probe and the corresponding free-stream parameters are shown for a range of free-stream and local flow variables.

SYMBOLS

Physical quantities in this report are given in the International System of Units (SI) and parenthetically in U.S. Customary Units. The measurements were made in U.S. units. Factors relating the two systems are presented in reference 3.

a	speed of sound, m/sec (ft/sec)
f	frequency, Hz
g	acceleration due to gravity, kg-m/N-sec^2 (32.2 lbm-ft/lbf-sec^2)
H	enthalpy, J/kg (BTU/lbm)
h	geometric altitude, m (ft)
J	mechanical equivalent of heat, N-m/J (778 ft-lbf/BTU)
M	Mach number
p	static pressure, kN/m^2 (lbf/ft^2)
p_i	stagnation pressure, kN/m^2 (lbf/ft^2)
T	temperature, °K (°R)
t	time, min or sec
V	velocity, m/sec (ft/sec)
$\dot{w}$	unit weight flow, kg/m^2-sec (lbm/ft^2-sec)
α	angle of attack, deg
ρ	density, kg/m^3 (lbm/ft^3)
Subscripts:	
b	base behind temperature probe package
bn	ball nose
c	location close to fluidic oscillator cavity
fo	fluidic oscillator
l	local conditions in front of temperature probe package
max	maximum
p	location close to piezoelectric pressure transducer

st	shielded thermocouple
t	calculated free-stream total condition
∞	free-stream condition

X-15 AIRPLANES AND LOCATION OF THE TEMPERATURE PROBE PACKAGE

The X-15 rocket-powered research airplanes could be tested over a wide range of total temperatures because they were capable of flight from subsonic to hypersonic speeds. The data of this report were obtained from flights involving the basic X-15 (X-15-1) airplane and an advanced version, designated the X-15-2. A photograph of the X-15-1 airplane is shown in figure 1, and a three-view drawing is shown in figure 2. Dimensional details are presented in reference 4. Dimensional details of the X-15-2 are presented in reference 5.

On both airplanes the temperature probe package was on top of the upper vertical fin at the leading edge (fig. 2). In this location the package was free from vehicle boundary layers, but was subject to shock wave impingement from shock waves generated from upstream portions of the airplane. Shock wave impingement would cause local flow parameters to deviate from free-stream values, except for local total temperature, which would remain essentially the same as free-stream total temperature. As shown in figure 3, a fluidic oscillator temperature probe, a shielded thermocouple temperature probe, and a pitot tube were installed in the front portion of the package. Additional installation details are given in reference 2.

TESTS

The X-15 was air launched from a B-52 airplane for the four flights discussed in this report. These flights, A, B, C, and D, are listed in the following table with corresponding maximum values of M, h, and T at which data were obtained.

Flight	Airplane	M_{max}	h_{max}, m (ft)	$(T_t)_{max}$, °K (°R)	Remarks
A	X-15-2	6.7	31,000 (102,000)	2014 (3625)	Fluidic oscillator and shielded thermocouple probe data obtained during portions of ascent.
B	X-15-1	4.8	38,750 (127,100)	1250 (2250)	Fluidic oscillator and shielded thermocouple probe data obtained during portions of ascent and descent.
C	X-15-1	5.0	36,950 (121,200)	1310 (2358)	Only shielded thermocouple probe data obtained during portions of ascent and descent.
D	X-15-1	5.4	32,800 (107,600)	1412 (2541)	Only fluidic oscillator probe data obtained during portions of ascent and descent.

The temperature probe package was first flown on the X-15-2 airplane on flight A. Data from this flight were published in reference 2. Both probes were adversely affected near the peak Mach number of the flight by high aerodynamic heating. The shielded thermocouple probe failed structurally because the temperatures experienced were well over its design limit. The fluidic oscillator probe is believed to have functioned during the high heating period; however, the heating degraded the signal from the piezoelectric pressure transducer which measured the probe output frequency, and about 10 to 15 seconds after peak Mach number was reached the signal was lost. Postflight examination showed that the probe shroud was oxidized.

Subsequent tests of the temperature probe package were made with the X-15-1 airplane, using additional probes of the same type and improved instrumentation. Data from flights B, C, and D were obtained from these X-15-1 flights.

Launch occurred at a free-stream Mach number of approximately 0.8 and a nominal altitude of 13,700 meters (45,000 feet). Free-stream total temperature at launch was approximately 244° K (439° R). A flight typically consisted of a powered ascent to rocket engine burnout followed by an unpowered descent. During the ascent, Mach number, altitude, and total temperature increased rapidly. Fluidic oscillator temperature probe data were obtained during portions of the ascent in flights A, B, and D, and shielded thermocouple temperature probe data were obtained during portions of the ascent in flights A, B, and C. During the unpowered descent, Mach number, altitude, and total temperature decreased steadily. In the descent, fluidic oscillator temperature probe data were obtained during portions of flights B and D; shielded thermocouple temperature probe data were obtained during portions of flights B and C.

During the flights, angle of attack varied from approximately 0° to approximately 20°, but angle of sideslip was essentially zero. The small vertical tail motions experienced during the flights are not believed to have affected the data obtained.

TEMPERATURE PROBES AND INSTRUMENTATION

Temperature

Fluidic oscillator probe.– Fluidic oscillator temperature probes are bistable fluid amplifiers. They sense total temperature of the ingested air by self-oscillation, which is induced by feeding back a portion of the output flow to modulate the input flow. The self-induced oscillation is approximately proportional to the square root of the absolute temperature of the ingested air. Figure 4 shows details of the fluidic oscillator temperature probe which was tested. Figure 4(a) is a photograph and figure 4(b) is a cutaway schematic of essential design features and airflow paths. Air, essentially at local stagnation conditions, enters the sensor inlet port, passes through the oscillator cavity, and is channeled rearward and exhausted through the sensor exhaust port. Incoming air is also channeled between the oscillator cavity body and the circular shroud to reduce heat loss from the oscillator cavity to the atmosphere.

The high-frequency pressure fluctuations generated by airflow through the oscillator cavity are propagated through the pressure signal line to the piezoelectric pressure transducer. The relationship between frequency, f, in hertz and temperature, T_{fo}, in ° K (° R) is given by the expression

$$T_{fo}\ (^\circ\ K) = 2.0713 \times 10^{-7}\ f^{2.0855} \quad (T_{fo}\ (^\circ\ R) = 3.7283 \times 10^{-7}\ f^{2.0855}) \qquad (1)$$

This equation was obtained from calibrations discussed in references 2 and 6. Reference 6 also presents descriptive and operational details of the fluidic oscillator probe.

The vacuum pump connection shown in figure 4(b) was used to supply a laboratory vacuum source to induce flow through the probe for ground tests and calibrations. A vacuum was not needed for the flight tests, because, in most instances, aircraft motion provided enough pressure differential across the probe to cause self-oscillation and generate a signal. The vacuum connection was capped during flight.

Figure 4(c) shows the components in the cooling loop, which used a mixture of water and glycol to cool the piezoelectric pressure transducer for flight A. Spent coolant was exhausted overboard. Also shown in figure 4(c) is the signal conditioning box, which fed the probe output frequency from the pressure transducer to the onboard tape recorder.

A pair of chromel-alumel thermocouples measured temperatures at two locations on the fluidic oscillator temperature probe. The approximate locations of these thermocouples are shown in figure 4(b). The thermocouple installed near the oscillator cavity to measure the approximate oscillator cavity temperature indicated the heat transfer from the incoming air to the oscillator cavity walls. The thermocouple positioned near the piezoelectric transducer monitored the approximate transducer temperature.

Shielded thermocouple probe.– Details of the shielded thermocouple probe which was tested are shown in figures 5(a) and 5(b). The probe is uncooled. Air entering the probe is at essentially local stagnation conditions and flows around the platinum versus platinum-10-percent-rhodium junction and through the annular paths formed by the three radiation shields. All air leaves the probe through the air exit ports. The probe was designed to have less than 2-percent error between Mach numbers of 3 and 5 and to be suitable for temperatures up to 1773° K (3191° R) (ref. 1).

Additional descriptive and operational details regarding the shielded thermocouple temperature probe are given in references 2 and 7.

Recording.– The fluidic oscillator temperature probe used a quartz piezoelectric transducer to measure the high-frequency acoustic signals generated in one of the two feedback paths of the sensor (ref. 2). These frequencies ranged from approximately 22,000 hertz to approximately 62,000 hertz. The diagram in figure 4(b) shows the transducer location and the pressure signal line. In flight A a transducer was used which had a pressure range of 0.69 kN/m^2 (0.1 lbf/in^2) to 2070 kN/m^2 (300 lbf/in^2) and a temperature range of 5.6° K (10° R) to 534° K (961° R). In flights B, C, and D a transducer was used which had extended temperature and pressure ranges, to 1090° K (1962° R) and 20,700 kN/m^2 (3000 lbf/in^2), respectively. The frequency measurements were recorded on an onboard tape recorder, as shown in figure 4(c). The data processing sequence used to obtain the measured frequency following each flight is described in reference 2. On some flights, low signal-to-noise ratio degraded the quality of the probe output signal, creating difficulties in obtaining the probe output frequency. Equation (1) was used to obtain the temperature, T_{fo}, from the measured frequency.

The voltage outputs of the chromel-alumel thermocouples and the shielded thermocouple temperature probe were individually combined with the voltage outputs of the reference thermocouples. The resulting voltages were fed directly into a 36-channel oscillograph. (Figure 5(b) illustrates the hookup for the shielded thermocouple probe. The reference thermocouple was installed in an electrically heated oven with a controlled temperature of approximately 343° K (617° R). The temperature of the reference thermocouple was monitored by a bead thermistor. The output of the thermistor was also recorded on the oscillograph. The recording system for the shielded thermocouple probe was designed for optimum operation at Mach numbers greater

than approximately 2.0, thus its operation at lower Mach numbers was marginal.

Pressures and Free-Stream Quantities

The pitot tube shown in figure 3 measured the stagnation pressure, p_{i_l}, experienced by both temperature probes. A static-pressure port was installed at the rear of the package close to the discharge port of the fluidic temperature probe to measure base pressure, p_b. These two pressures provided both the pressure drop and the pressure ratio across the temperature probe package during a flight. Both pressures were measured by 138 kN/m^2 (20 lbf/in^2) unbonded strain gage absolute-pressure transducers. These transducers were installed within the temperature probe package, which permitted the use of short tubing lengths to the sensing ports. Signals from the pressure transducers were recorded on the oscillograph.

The hemispherical flow direction sensor (ball nose) shown at the nose of the airplane in figure 1 was used on both airplanes. This sensor measured free-stream angle of attack, angle of sideslip, and stagnation pressure. Free-stream Mach number, velocity, altitude, temperature, and angle of attack were determined from flow-direction-sensor data, radar tracking, meteorological soundings, and other inputs. The techniques used to obtain these parameters are discussed in reference 1. Free-stream density, ρ_∞, was obtained from the standard altitude table for the test altitude (ref. 8). For some of the altitude test points in this report, which were above approximately 35,000 meters (115,000 feet), values of free-stream temperature, T_∞, obtained from the meteorological soundings were not used because of large measurement uncertainties. For these points the standard atmosphere values for the test altitude were assumed (ref. 8).

ANALYSIS

Probe Behavior

The analyses in references 6 and 9 and the specifications of reference 7 show that the transfer functions of the fluidic oscillator and the shielded thermocouple probe are essentially first-order lag functions. The major cause of the lag in both probes is the time it takes for the sensing element to establish thermal equilibrium with the incoming air. Response of these probes to linear or ramp inputs of temperature is a parallel ramp output which lags the ramp input by a relatively constant time interval. The X-15 trajectories generated ramp inputs in T_t during the ascent and descent, as discussed in the RESULTS AND DISCUSSION section. Consequently, the parallelism between T_t and T_{fo} and between T_t and T_{st} was the principal criterion used in establishing that each probe was operating properly.

Probe response was determined by comparing T_t with T_{fo} and T_t with T_{st} in time history plots of individual flights. Both probes responded with ramp outputs parallel to the ramp input of T_t during portions of the ascent and descent trajectories. For the fluidic oscillator probe, high values of unit weight flow, $\dot{w}_\infty$, or local stagnation pressure, p_{i_l}, generally indicated flight regions of parallelism with T_t. Values of $\dot{w}_\infty$ of approximately 30 ±6 kg/m^2-sec (6.1 ±1.2 lbm/ft^2-sec) appeared to be the lower limit of this occurrence. For the shielded thermocouple probe, free-stream Mach numbers greater than approximately 2.0, together with p_{i_l} values greater than about 9.6 kN/m^2 (200 lbf/ft^2), generally indicated flight regions for parallelism with T_t.

In addition to the parallelism criterion for the fluidic oscillator probe, before using the probe test data (ref. 6), it was also necessary to establish that airflow through the probe was choked. This criterion was established by using the data in figure 6, a plot of $|T_t - T_{fo}|$ from flights B and D against the ratio p_{il}/p_b for $\dot{w}_\infty$ greater than approximately 49 kg/m^2-sec (10 lbm/ft^2-sec). As p_{il}/p_b decreases below values from 3.0 to 4.5, $|T_t - T_{fo}|$ becomes large despite the fact that $\dot{w}_\infty$ is high. The large increase in $T_t - T_{fo}$ is attributed to the unchoking of the probe airflow at the exit of the oscillator cavity. Evidence of unchoking occurred at free-stream Mach numbers below approximately 0.8 to 1.2; above $M_\infty = 1.2$, the probe was always choked.

During the descent in flights B and D, sharp pressure spikes in p_{il} were noted in the time history plots. These pressure spikes were attributed to the impingement on the temperature probe package of shock waves originating from upstream portions of the airplane. Reference 10 discusses similar impingement on the underside of the X-15-2 airplane. Temperature probe data obtained during shock wave impingement generally did not satisfy the parallelism criterion.

Calculated Parameters

In addition to the measured parameters discussed in the TEMPERATURE PROBES AND INSTRUMENTATION section, parameters were needed to analyze and interpret data from the two total temperature probes. Calculated free-stream total temperature, T_t, was obtained by means of the energy equation:

$$H_t = H_\infty + \frac{V_\infty^2}{2gJ} \tag{2}$$

in which H_∞ was obtained from the measured or assumed value of T_∞ and the tables of reference 11. After H_t was calculated from equation (2), reference 11 was used to obtain T_t.

The quantities V_{fo} and V_{st} were calculated from the following equations:

$$V_{fo} = [(H_{fo} - H_\infty)2gJ]^{1/2} \tag{3}$$

$$V_{st} = [(H_{st} - H_\infty)2gJ]^{1/2} \tag{4}$$

The quantities H_{fo} and H_{st} were calculated from reference 11 by using the measured values of T_{fo} and T_{st}. The quantities M_{fo} and M_{st} were calculated from the following equations:

$$M_{fo} = V_{fo}/a_\infty \tag{5}$$

$$M_{st} = V_{st}/a_\infty \tag{6}$$

Unit weight flow was calculated from the expression

$$\dot{w}_\infty = \rho_\infty V_\infty \tag{7}$$

The thermal analysis of reference 6 shows that a high heat transfer rate from the incoming air to the oscillator cavity improves the response and accuracy of the fluidic oscillator probe. For a probe of a given size, the analysis indicates a high heat transfer rate if airflow through the probe and the heat transfer coefficient are high. It was not

possible to calculate the actual airflow through the probe or the heat transfer coefficient with certainty from the available measurements. However, $\dot{w}_\infty$ is an approximate measure of the actual heating effect of the unit airflow passing through the probe. This statement follows from the close agreement of flight values of p_{ibn} and p_{il}; an example of this agreement is presented later. Consequently, $\dot{w}_\infty$ was used to analyze data from the fluidic oscillator probe.

ERRORS

The estimated errors in measured and calculated parameters are as follows:

Parameter	Estimated error
f	±200 Hz
M_∞	±0.05 (ref. 1)
V_∞	±15 m/sec (±50 ft/sec) (ref. 1)
h	±150 m to ±300 m (±500 ft to ±1000 ft) (ref. 1)
p_{ibn}	±0.41 kN/m² (±8.5 lbf/ft²)
T_∞	±0.7° K (±1.3° R) (ref. 1)
α	±0.25°
$\dot{w}_\infty$	±0.88 kg/m²-sec (±0.18 lbm/ft²-sec)
p_{il}	±1.4 kN/m² (±30 lbf/ft²)
p_{ib}	±1.4 kN/m² (±30 lbf/ft²)
T_c	±6° K (±11° R)
T_p	±6° K (±11° R)
V_{fo}	±9 m/sec (±30 ft/sec)
V_{st}	±9 m/sec (±30 ft/sec)
M_{fo}	±0.03
M_{st}	±0.03

These estimated errors include instrument errors, reading errors, and calculation errors. The several errors were combined in a root-sum-square technique to obtain the listed errors. Figure 7 presents the variation of the estimated errors in T_t, T_{fo}, and T_{st} as a function of T_t. Errors in T_{fo} and T_{st} change only slightly as T_t increases over the test range. The estimated error in T_t shows a steady increase as T_t increases. This results primarily from the ±15 m/sec (±50 ft/sec) error in V_∞, with little effect of the error in T_∞ of ±0.7° K (±1.3° R)

(eq. (2)).

RESULTS AND DISCUSSION

Time Histories

Figure 8 is a time history of the measured and calculated parameters for flight A, representing the rocket-powered ascent portion of the flight. In figure 8(a), a rapid buildup in free-stream Mach number to 6.7 and altitude to 31,000 meters (102,000 feet) is shown along with accompanying changes in angle of attack, α, and ambient temperature, T_∞. Figure 8(a) also shows flow-direction-sensor stagnation pressure, p_{ibn}, and unit weight flow, $\dot{w}_\infty$, which show similar variations. Total temperatures, T_t, T_{fo}, and T_{st}, are shown in figure 8(b). The fluidic oscillator probe shows parallelism with the ramp variation of T_t for most of the powered portion of the flight. The shielded thermocouple probe begins to show parallelism with T_t about 1.4 minutes after launch and continues to the end of the powered portion of the flight. The beginning of parallelism in the data is associated with operation above approximately $M_\infty = 2.0$.

Figure 9 is a time history of flight B. Figure 9(a) shows that a peak altitude of approximately 67,500 meters (221,500 feet) was reached and that a Mach number of approximately 4.8 to 5.0 was maintained during the middle portion of the flight. The accompanying changes in angle of attack are also shown. Angles of attack near 20° were reached during the descent.

Measured stagnation pressures, p_{ibn} and p_{il}, base pressure, p_b, and calculated unit mass flow, $\dot{w}_\infty$, are also presented in figure 9(a). Simultaneous relative peaks in p_{ibn}, p_{il}, and $\dot{w}_\infty$ are reached in both the ascent and descent portions of the flight, whereas all quantities decrease to near zero at an altitude above approximately 60,000 meters (197,000 feet). The sharp pressure spikes in p_{il} between 4.0 minutes and 4.5 minutes after launch are attributed to shock wave impingement during the high angle of attack portion of the descent maneuver.

Figure 9(b) presents measured and calculated temperatures for flight B. Standard atmospheric values of T_∞ were used during the middle portion of the flight when the altitude was too high for meteorological soundings to be made. Variations in T_t resemble the variations in M_∞ shown in figure 9(a) and are considered to be ramp variations. During the middle portion of the flight, T_{st} shows extremely poor agreement with T_t; whereas the fluidic oscillator showed no output between about 1 minute 10 seconds and 4 minutes after launch because of near-zero values of pressure, p_{il}, and flow, $\dot{w}_\infty$. During ascent, parallelism between the T_t and T_{fo} traces and the oscillator cavity temperature, T_c, is closely associated with high values of $\dot{w}_\infty$ or p_{il}. The relationship between the three temperatures is similar during descent after the period of shock wave impingement.

For the shielded thermocouple probe, T_{st} and T_t remain parallel and agree closely at high values of p_{il}, as suggested in reference 7. However, T_{st} and T_t are not parallel at low free-stream Mach numbers at the beginning of the ascent and at the end of the descent. These results are similar to those noted in flight A and are believed to be caused primarily by the limitations of the probe recording system mentioned previously. Both probes are affected by shock wave impingement in the period between 4.0 minutes and 4.5 minutes after launch.

Time histories such as those in figures 8 and 9 provide insight regarding relationships between test variables. For example, p_{ibn} and p_{il} showed close agreement for flights B, C,

and D. The flow variables most affecting the fluidic oscillator temperature probe appeared to be T_t, $\dot{w}_\infty$, p_{i_l}, and p_b. The flow variables most affecting the shielded thermocouple temperature probe appeared to be T_t and p_{i_l}. The quantities M_∞, T_∞, and h_∞ affected both probes indirectly, through effects on T_t, $\dot{w}_\infty$, and p_{i_l}. Angle of attack appeared to have no effect on the probes except when it combined with high free-stream Mach number to cause shock wave impingement during descent.

For Mach numbers between 1.2 and 6.7 and unit mass flow equal to or greater than 30 ±6 kg/m²-sec (6.1 ±1.2 lbm/ft²-sec), the fluidic oscillator probe temperature, T_{fo}, was parallel to ramp changes in total temperature, T_t. For Mach numbers between approximately 2.0 and 6.7 and local stagnation pressure greater than 9.6 kN/m² (200 lbf/ft²), the shielded thermocouple probe temperature, T_{st}, was also parallel to ramp changes in total temperature.

Fluidic Oscillator Probe

In figures 10 to 16, air-data parameters T_{fo}, V_{fo}, and M_{fo} obtained from the fluidic oscillator probe are plotted as functions of the free-stream parameters T_t, $\dot{w}_\infty$, V_∞, and M_∞. Data are presented for both ascending and descending flight and include variations in M_∞, h_∞, and α. Figure 10 shows the variation of T_{fo} with T_t for approximately constant values of $\dot{w}_\infty$. Values of $\dot{w}_\infty$ increase uniformly from 30 ±6 kg/m²-sec (6.1 ±1.2 lbm/ft²-sec) in figure 10(a) to 114 ±6 kg/m²-sec (23.4 ±1.2 lbm/ft²-sec) in figure 10(h). The data are faired linearly in figures 10(b) to 10(h). The data fairing in figure 10(a) is quasi-linear because of the low value of unit weight flow 30 ±6 kg/m²-sec (6.1 ±1.2 lbm/ft²-sec), which is only marginal for establishing good probe operation. In each part of figure 10, the faired lines show increasing departure from the line of perfect agreement with increasing T_t. This departure is considered to be fluidic oscillator probe error and is related to both $\dot{w}_\infty$ and T_t. Thus, the data indicate that the error increases with T_t for a given $\dot{w}_\infty$ and decreases with increase in $\dot{w}_\infty$ for a given T_t.

This relationship is shown again in figure 11, a plot of $T_t - T_{fo}$ against T_t for approximately constant values of $\dot{w}_\infty$. The data were obtained from figure 10. The quantity $T_t - T_{fo}$ varies linearly with T_t for all values of $\dot{w}_\infty$ except 30 ±6 kg/m²-sec (6.1 ±1.2 lbm/ft²-sec). The figure indicates that low values of $T_t - T_{fo}$ can be obtained if $\dot{w}_\infty$ can be kept high. For example, at T_t = 1200° K (2160° R) for $\dot{w}_\infty$ = 90 ±6 kg/m²-sec (18.4 ±1.2 lbm/ft²-sec), $T_t - T_{fo}$ = 30° K (54° R).

A convenient way to present the test data to show the effect of $\dot{w}_\infty$ is to plot the fractional error, $\frac{T_t - T_{fo}}{T_t}$, against $\dot{w}_\infty$, as shown in figure 12. Data were obtained from figure 11 by averaging the computed values of $\frac{T_t - T_{fo}}{T_t}$ for several temperatures on each of the $\dot{w}_\infty$ curves. In this plot all the test data are included in a single curve. As expected, the fractional error becomes small asymptotically with increasing weight flow. Fractional errors are approximately 0.02 or less for $\dot{w}_\infty$ greater than approximately 90 kg/m²-sec (18.4 lbm/ft²-sec).

The parametric analyses for velocity, V_{fo}, and Mach number, M_{fo}, were performed similarly to the analysis for T_{fo}, because V_{fo} and M_{fo} were calculated from T_{fo}. The results of the analyses are similar to the results obtained from T_{fo} in illustrating the effect of $\dot{w}_\infty$ on errors. For the prescribed $\dot{w}_\infty$ ranges, V_{fo} varied from 200 m/sec to 2100 m/sec (650 ft/sec to 6900 ft/sec), and M_{fo} ranged from 1.2 to 6.7.

Figure 13, a companion figure of figure 11, is a plot of $V_\infty - V_{fo}$ against V_∞ and figure 14, a companion figure of figure 12, is a plot of $\frac{V_\infty - V_{fo}}{V_\infty}$ against $\dot{w}_\infty$. Figures 15 and 16 show the Mach number errors and are companion figures of figures 11 and 12, respectively. Figures 14 and 16 show the asymptotic relation of $\frac{V_\infty - V_{fo}}{V_\infty}$ and $\frac{M_\infty - M_{fo}}{M_\infty}$ with the unit weight flow that was shown by $\frac{T_\infty - T_{fo}}{T_\infty}$ in figure 12.

Shielded Thermocouple Probe

The shielded thermocouple probe temperature, T_{st}, and the calculated real gas total temperature, T_t, data are compared in figure 17. The data represent conditions of M greater than approximately 2.0 and p_{i_l} greater than approximately 9.6 kN/m² (200 lbf/ft²). The temperature range extends from about 375° K (675° R) to the maximum temperature tested, 2014° K (3625° R), which was well in excess of the probe design temperature of 1773° K (3191° R). The bulk of the data extends from about 375° K (675° R) to about 1300° K (2340° R), with a corresponding Mach number variation from 2.0 to approximately 5.0. Data above 1300° K (2340° R) are limited to those obtained from flight A. Data at temperatures below 1300° K (2340° R) are on both sides of the perfect agreement line and show randomness. Although more data above 1300° K (2340° R) would be desirable, agreement between T_{st} and T_t is considered to be good over the temperature range shown.

The data of figure 17 are plotted as $|T_t - T_{st}|$ versus T_t in figure 18. The sum of the estimated measurement error in T_{st} and the calculated error in T_t is shown as a dashed line. Most of the data points fall randomly below the dashed line and above zero error, indicating that the values of $|T_t - T_{st}|$ are due primarily to measurement errors. The data points above the dashed line are believed to be caused by measurement errors in excess of those estimated. Figures 17 and 18 show that T_{st} is essentially equal to T_t over the temperature range covered.

In figures 19 and 20 V_{st} is plotted against V_∞ and M_{st} is plotted against M_∞, respectively, similar to the manner in which the temperature data are shown in figure 17. Agreement between the parameters in both figures is good.

In figures 21 and 22, respectively, $|V_{st} - V_\infty|$ is plotted against V_∞ and $|M_{st} - M_\infty|$ is plotted against M_∞. Figures 19 to 22 indicate that, essentially, V_{st} equals V_∞ and M_{st} equals M_∞ over the test ranges shown.

Comparison of Air-Data Parameters for Both Probes

Air-data parameters derived from the two probes are compared in figure 23 on a Mach number-altitude background to indicate how they might be used on future vehicles. In this figure, probe-derived parameters are ratioed to corresponding radar-derived parameters. This procedure makes the radar-derived parameters, T_t, V_∞, and M_∞, standards for comparing both probes. The ratios shown can be used as correction factors to correct the probe-derived parameters to radar-derived parameters. In figure 23(a), both probe measurements are ratioed to T_t, in figure 23(b), to V_∞, and in figure 23(c), to M_∞.

For the fluidic oscillator probe the ratios, which were obtained from figures 12, 14, and 16, are shown for six constant values. The fractional errors $\frac{T_t - T_{fo}}{T_t}$, $\frac{V_\infty - V_{fo}}{V_\infty}$, and $\frac{M_\infty - M_{fo}}{M_\infty}$ are uniquely related to $\dot{w}_\infty$ in these figures. Therefore, lines of constant $\dot{w}_\infty$ plotted

on a Mach number-altitude background can be labeled as $\frac{T_t - T_{fo}}{T_t}$, $\frac{V_\infty - V_{fo}}{V_\infty}$, and $\frac{M_\infty - M_{fo}}{M_\infty}$, or with slight manipulation as $\frac{T_{fo}}{T_t}$, $\frac{V_{fo}}{V_\infty}$, and $\frac{M_{fo}}{M_\infty}$. Ratios from 0.98 to 0.88 are shown; values below 0.88 are considered to be unreliable. The ratio curves are plotted from $M_\infty = 1.2$, the upper limit for the onset of choked flow through the probe, to $M_\infty = 6.7$, the Mach number test limit. Extending the curves over the entire Mach number range in figure 23 is equivalent to linearly extrapolating the $\dot{w}_\infty$ curves in figures 11, 13, and 15 over the entire test range of the abcissa. This extrapolation is believed to be valid.

For the shielded thermocouple probe, the ratios $\frac{T_{st}}{T_t} = 1.0$, $\frac{V_{st}}{V_\infty} = 1.0$, and $\frac{M_{st}}{M_\infty} = 1.0$ extend over a bounded region of the Mach number-altitude background (figs. 23(a), 23(b), and 23(c)). The Mach number limits extend from about 2 to 6. The lower boundary line corresponds to $p_{il} = 152$ kN/m^2 (3175 lbf/ft^2); the test limit for p_{il} occurred on flight C at $M_\infty = 4.2$. The upper boundary line corresponds to $p_{il} = 9.6$ kN/m^2 (200 lbf/ft^2); the test limit for p_{il} occurred on flight B at $M_\infty = 4.4$. The lower limit line and the upper limit line were both extrapolated to $M_\infty = 6$ and $M_\infty = 2$ from the test limit points. Accordingly, these lines may not represent the actual operational limits of the probe. In this region all correction factors are unity, or $\frac{T_{st}}{T_t} = 1.0$, $\frac{V_{st}}{V_\infty} = 1.0$, and $\frac{M_{st}}{M_\infty} = 1.0$.

Comparison of the correction factors for the two probes shows that both probes are suitable for measuring temperature in the Mach 6 temperature environment and that the shielded thermocouple probe has a wider altitude capability than the fluidic oscillator probe. At $M_\infty = 6$ the fluidic oscillator probe is limited to an altitude of about 29,000 meters (95,000 feet), whereas the shielded thermocouple probe can be used to slightly greater than 42,000 meters (138,000 feet). The structural integrity of the fluidic oscillator probe provides it with a wider Mach number capability than that of the shielded thermocouple probe. Below $M_\infty = 2$, the shielded thermocouple probe operation becomes marginal because of the design limitations of the probe and the recording system. The fluidic oscillator probe can be used to $M_\infty = 1.2$. The correction factor curves for the fluidic oscillator probe show only gradual changes and are easily applied over the ranges covered.

Future use of the fluidic oscillator probe is suggested for Mach numbers from approximately 1.2 to greater than 6. Future use of the shielded thermocouple probe is suggested for Mach numbers up to 6. These suggestions are only for the configurations tested. Versions of the present fluidic oscillator probe with redesigned oscillator cavities and cooling systems appear to have applications for higher temperatures and Mach numbers (ref. 12).

CONCLUSIONS

A fluidic oscillator temperature probe and a shielded thermocouple temperature probe were tested on the X-15 airplane over a rapidly changing environment which included flight at Mach 6.7 and a total temperature that reached 2014° K (3625° R). The following conclusions were reached:

1. Both probes were suitable for measuring temperature in the Mach 6 temperature environment; the fluidic oscillator probe appeared to have a capability for Mach numbers somewhat in excess of 6.

2. For Mach numbers between 1.2 and 6.7 and free-stream unit weight flow equal to or greater than 30 ±6 kg/m^2-sec (6.1 ±1.2 lbm/ft^2-sec), the fluidic oscillator probe temperature was parallel to ramp changes in total temperature. Under these conditions, the probe error increased with increasing total temperature and decreasing unit weight flow. Differences between probe-determined velocity and radar-determined velocity increased with increasing velocity and decreasing weight flow. Differences between probe-determined Mach number and radar-determined Mach number increased with increasing Mach number and decreasing weight flow.

3. For Mach numbers between approximately 2.0 and 6.7 and local stagnation pressure greater than 9.6 kN/m^2 (200 lbf/ft^2), the shielded thermocouple probe temperature was parallel to ramp changes in total temperature. Under these conditions the shielded thermocouple probe temperature and total temperature agreed and probe-determined velocity and Mach number agreed with radar-determined velocity and Mach number.

Flight Research Center,
National Aeronautics and Space Administration,
Edwards, Calif., December 10, 1971.

REFERENCES

1. Webb, Lannie D.: Characteristics and Use of X-15 Air-Data Sensors. NASA TN D-4597, 1968.

2. Bogue, Rodney K.; and Webb, Lannie D.: Advanced Air Data Sensing Techniques. Proceedings of the 5th International Aerospace Instrumentation Symposium, March 25–28, 1968, Cranfield, England, pp. 66-75.

3. Mechtly, E. A.: The International System of Units–Physical Constants and Conversion Factors. NASA SP-7012, 1969.

4. Anon.: Aerodynamic Dimensional Data for the X-15 Airplane (NAA Model Designation NA-240). Rep. No. NA-56-810, North American Aviation, Inc., July 10, 1956 (rev. Feb. 10, 1959).

5. Anon.: Aerodynamic Dimensional Data for the Advanced X-15A-2 Airplane. Rep. No. NA-56-810, Appendix B, North American Aviation, Inc., Dec. 16, 1963.

6. Bailey, R. G.; Sherwood, L. L.; Solie, K. E.; Starr, J. B.; and Zoerb, E. G.: A Study of All-Fluid, High-Temperature-Sensing Probes. Honeywell, Inc. (NASA CR-90092), 1967.

7. Anon.: Total Temperature Sensors. Bulletin 7637, Rev. B, Rosemount Engineering Co., 1963, p. 20.

8. Anon.: U.S. Standard Atmosphere, 1962. NASA, U.S. Air Force, U.S. Weather Bur., Dec. 1962.

9. Reilly, R. J.: A Survey of Fluidic Components and Their Application to Gas Turbine Control. Supersonic Turbo-jet Propulsion Systems and Components, J. Chauvin, ed., Ch. 7, AGARDograph 120, 1969, p. 379.

10. Burcham, F. W., Jr.; and Nugent, Jack: Local Flow Field Around a Pylon-Mounted Dummy Ramjet Engine on the X-15-2 Airplane for Mach Numbers From 2.0 to 6.7. NASA TN D-5638, 1970.

11. Keenan, Joseph H.; and Kaye, Joseph: Gas Tables–Thermodynamic Properties of Air Products of Combustion and Component Gases. John Wiley and Sons, Inc., N.Y., 1949.

12. Bailey, Ronald G.: High Total Temperature Sensing Probe for the X-15 Hypersonic Aircraft. Honeywell, Inc. (NASA CR-116772), 1968.

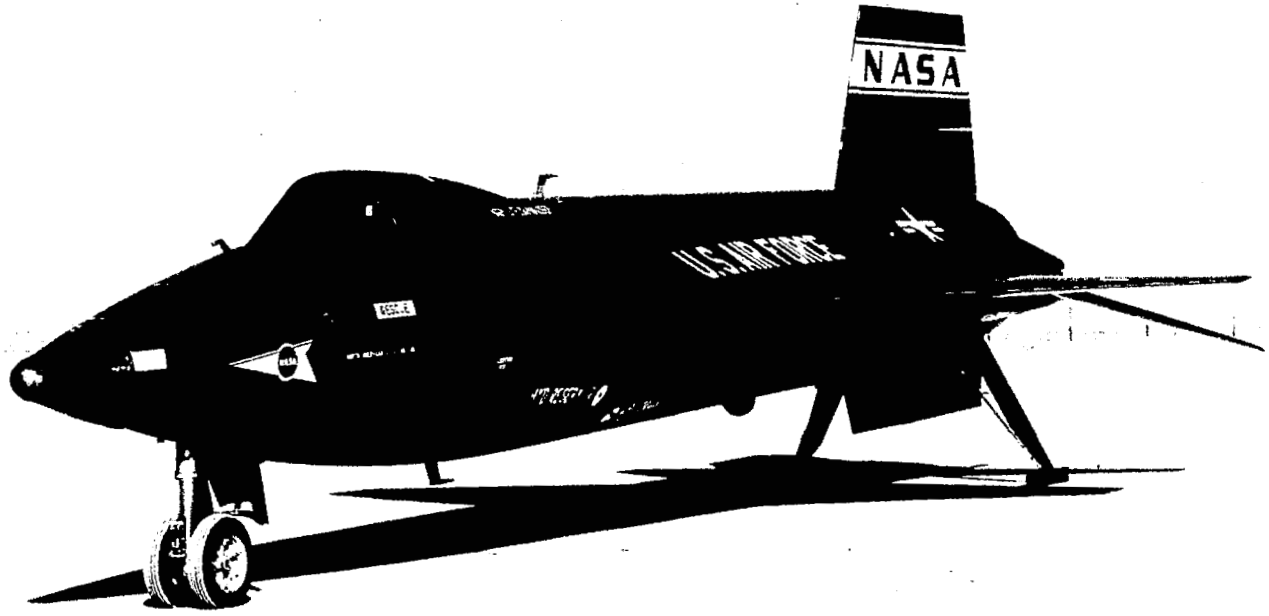

Figure 1. X-15-1 airplane. E-7902

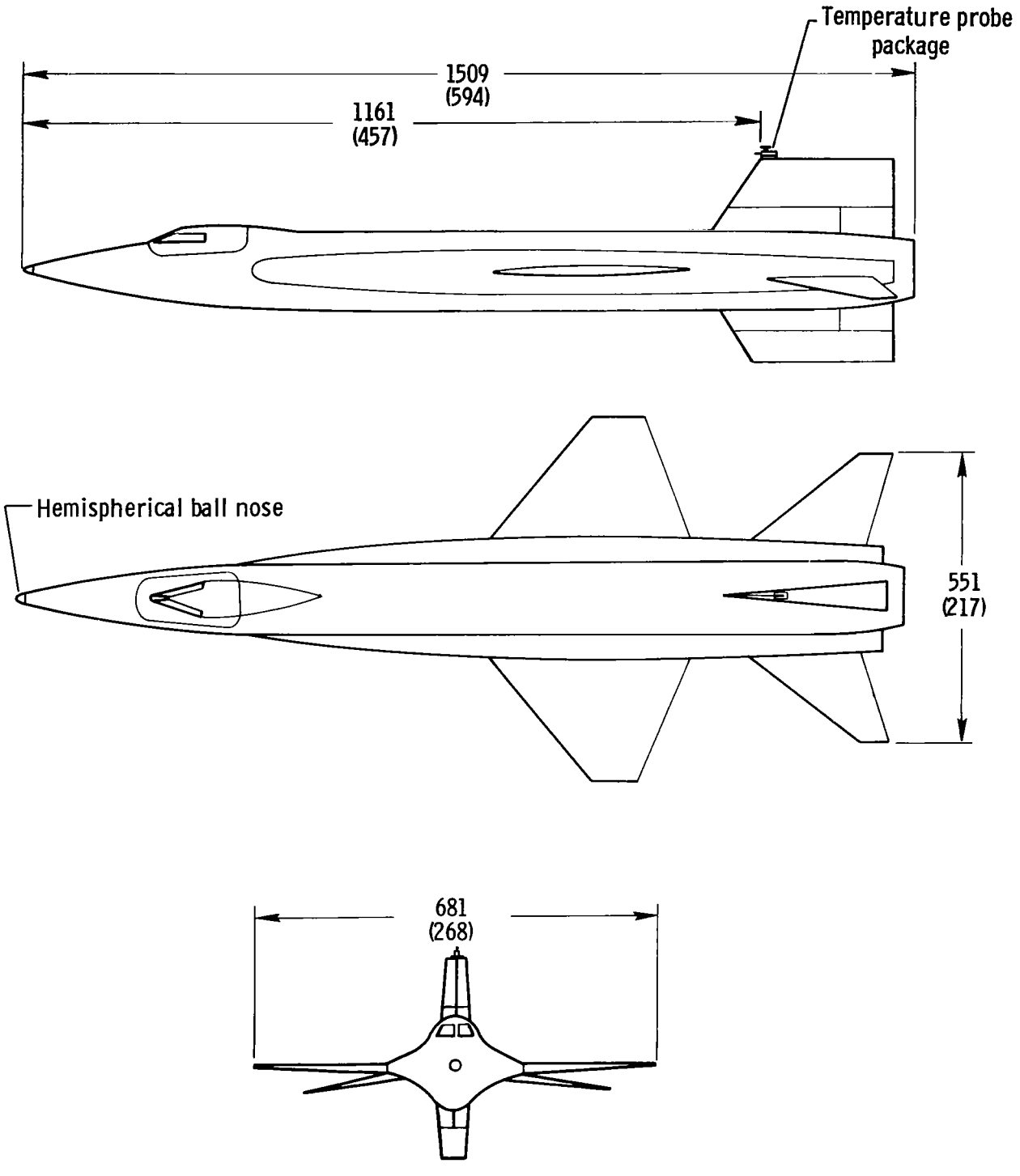

Figure 2. X-15-1 airplane showing the temperature probe package location. Dimensions in centimeters (inches).

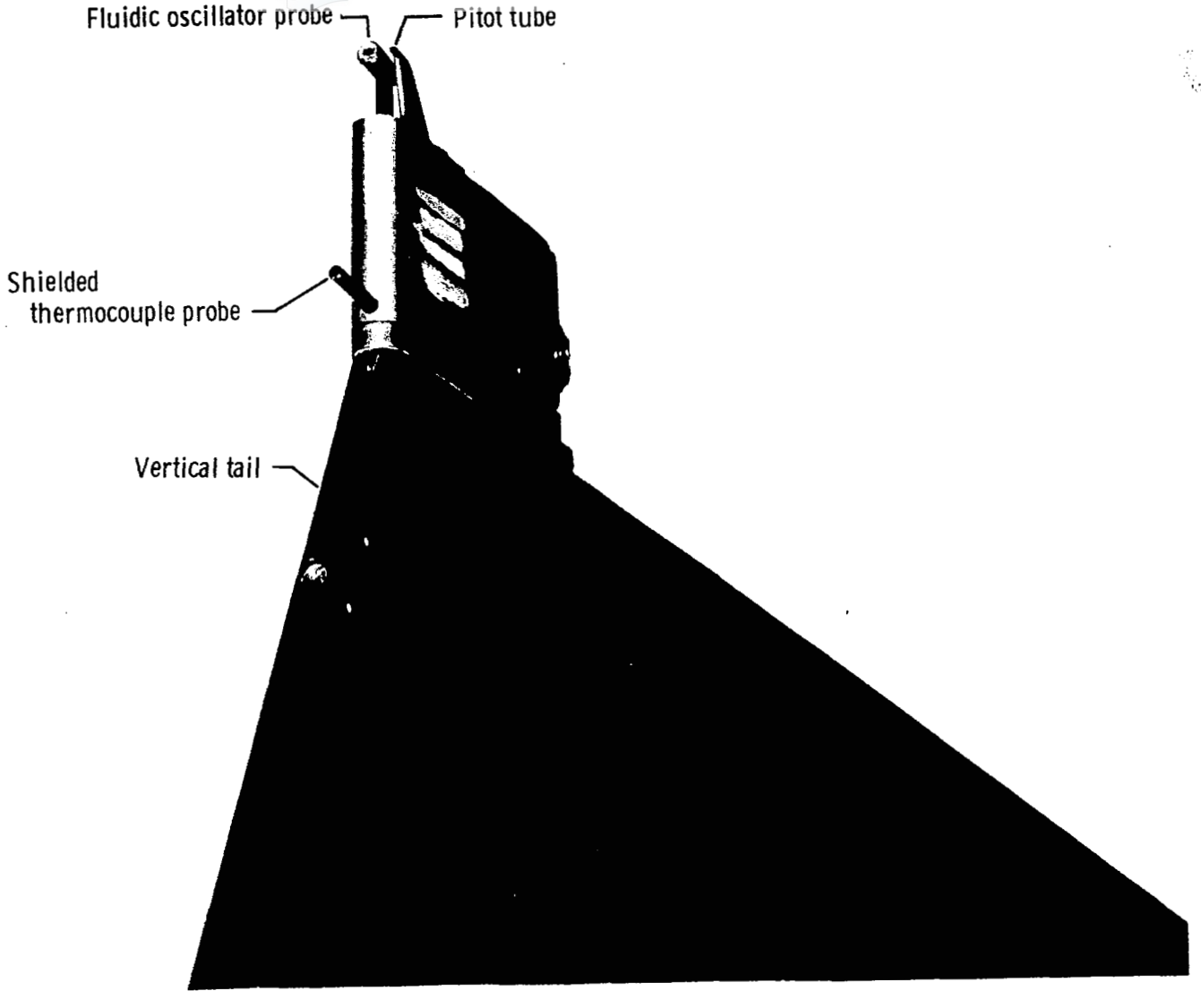

E-19081

(a) Closeup photograph.

Figure 3. Details of temperature probe package.

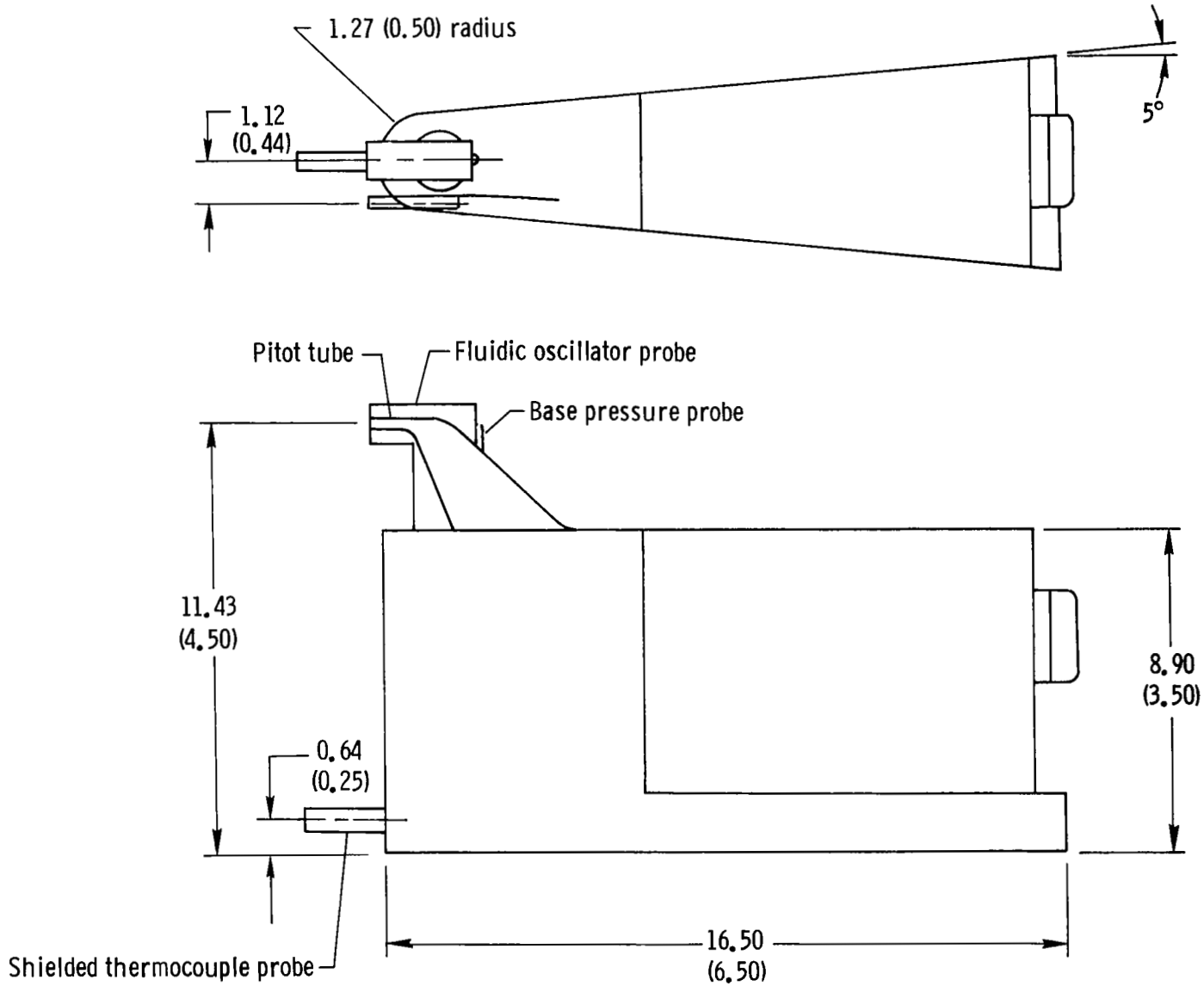

(b) Sketch showing dimensional details. Dimensions in centimeters (inches).

Figure 3. Concluded.

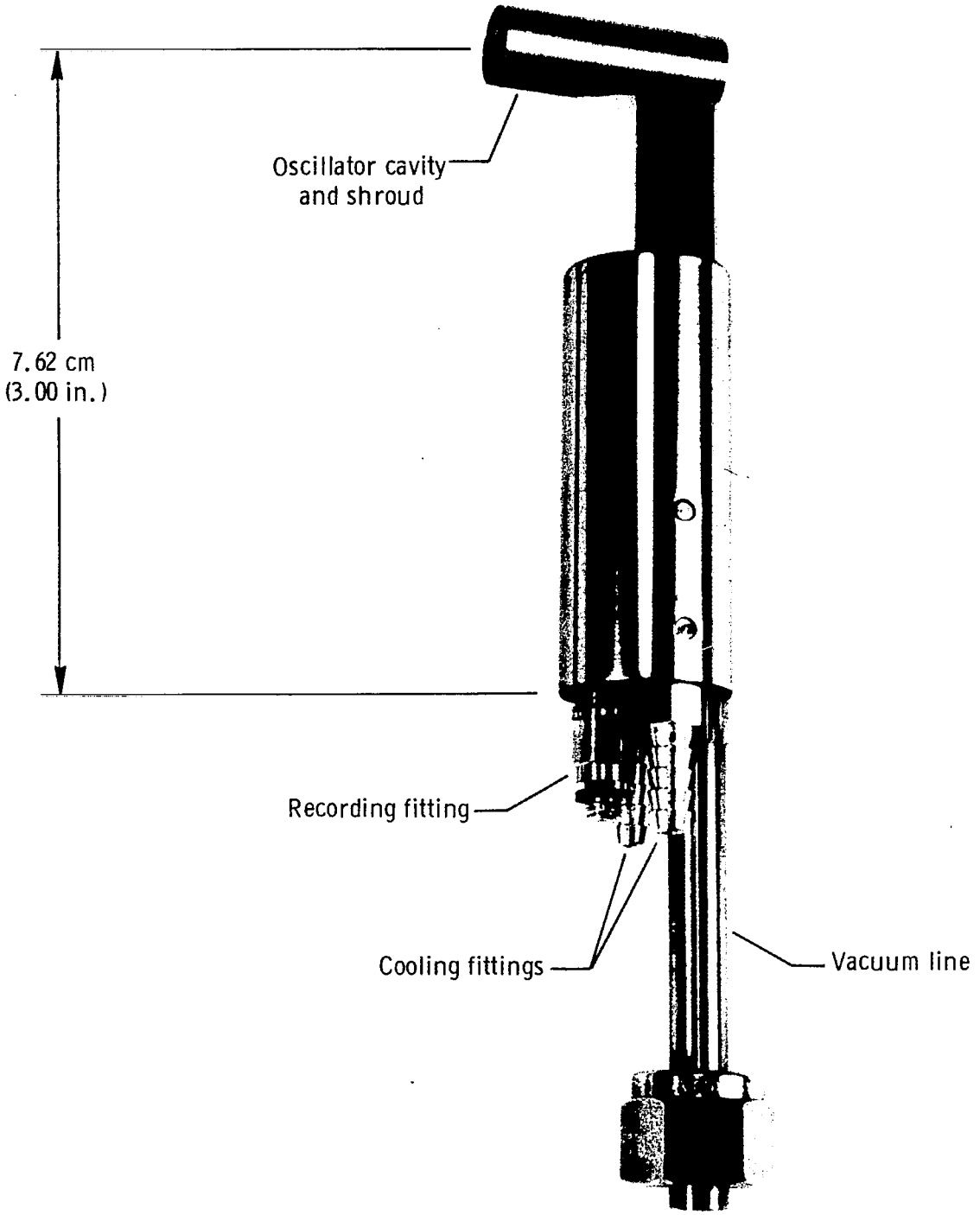

(a) Photograph. E-18365

Figure 4. Details of the fluidic oscillator temperature probe.

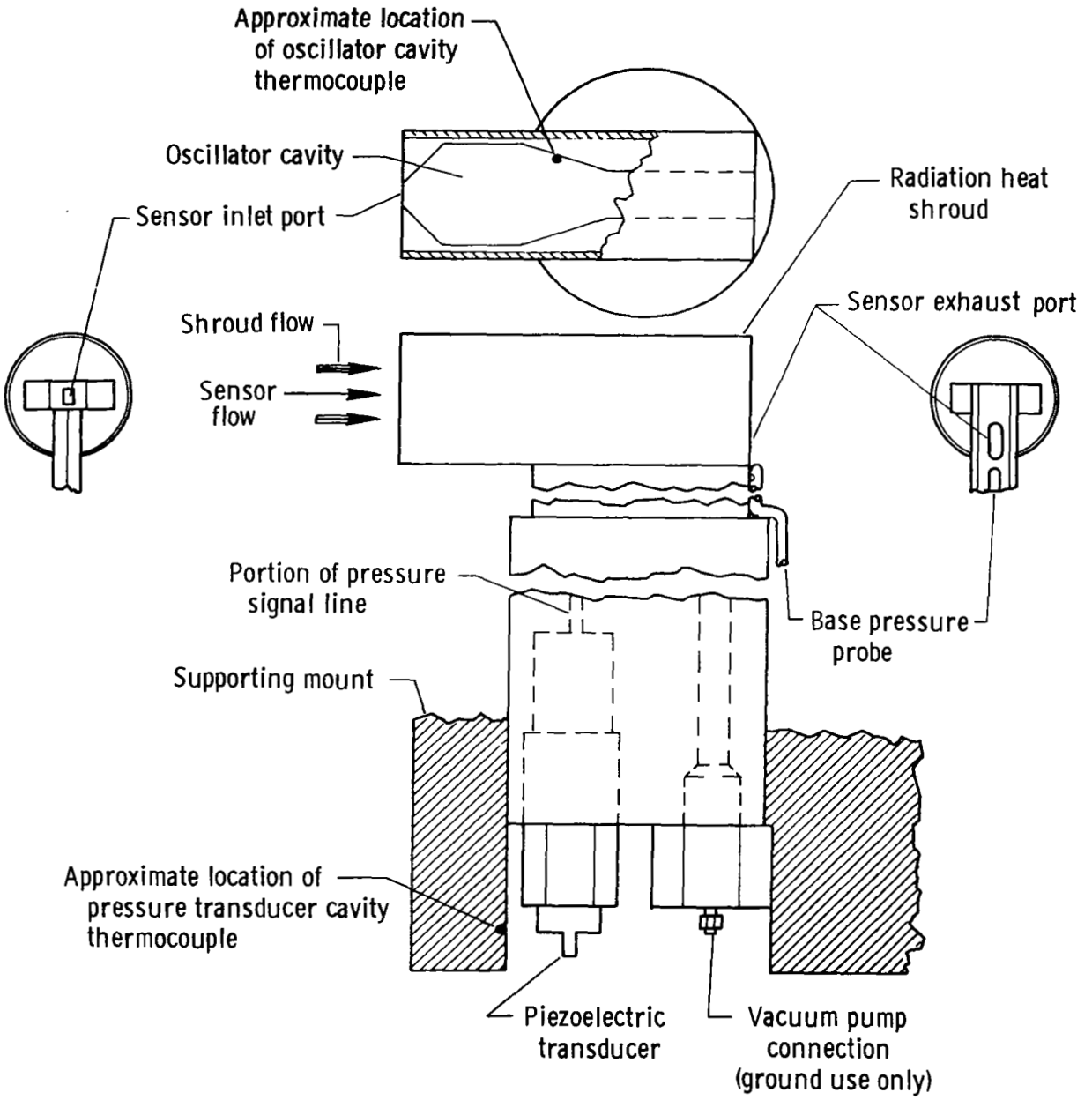

(b) Cutaway schematic diagram. (Drawing not to scale; cooling lines not shown.)

Figure 4. Continued.

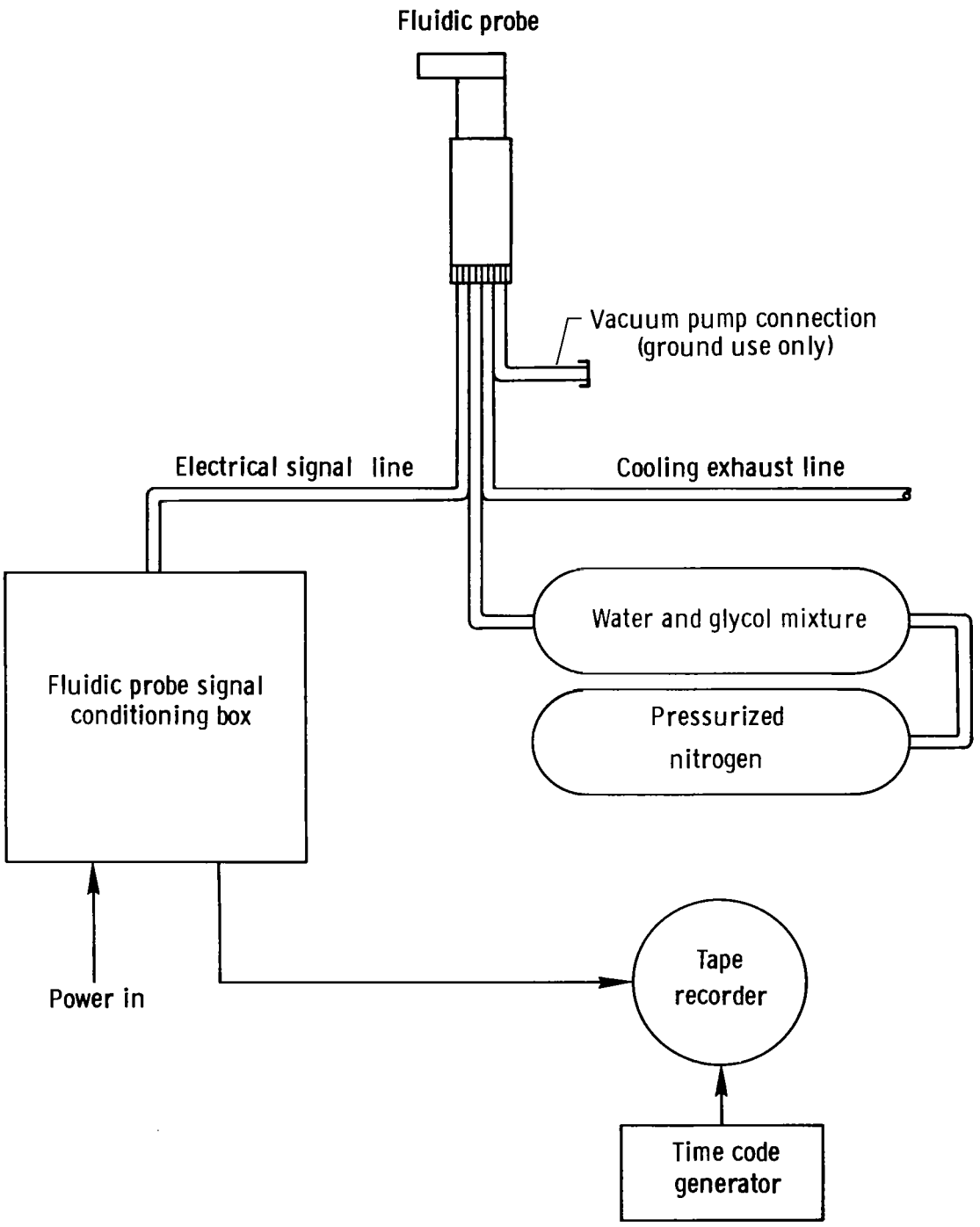

(c) Schematic diagram of cooling and frequency recording systems.

Figure 4. Concluded.

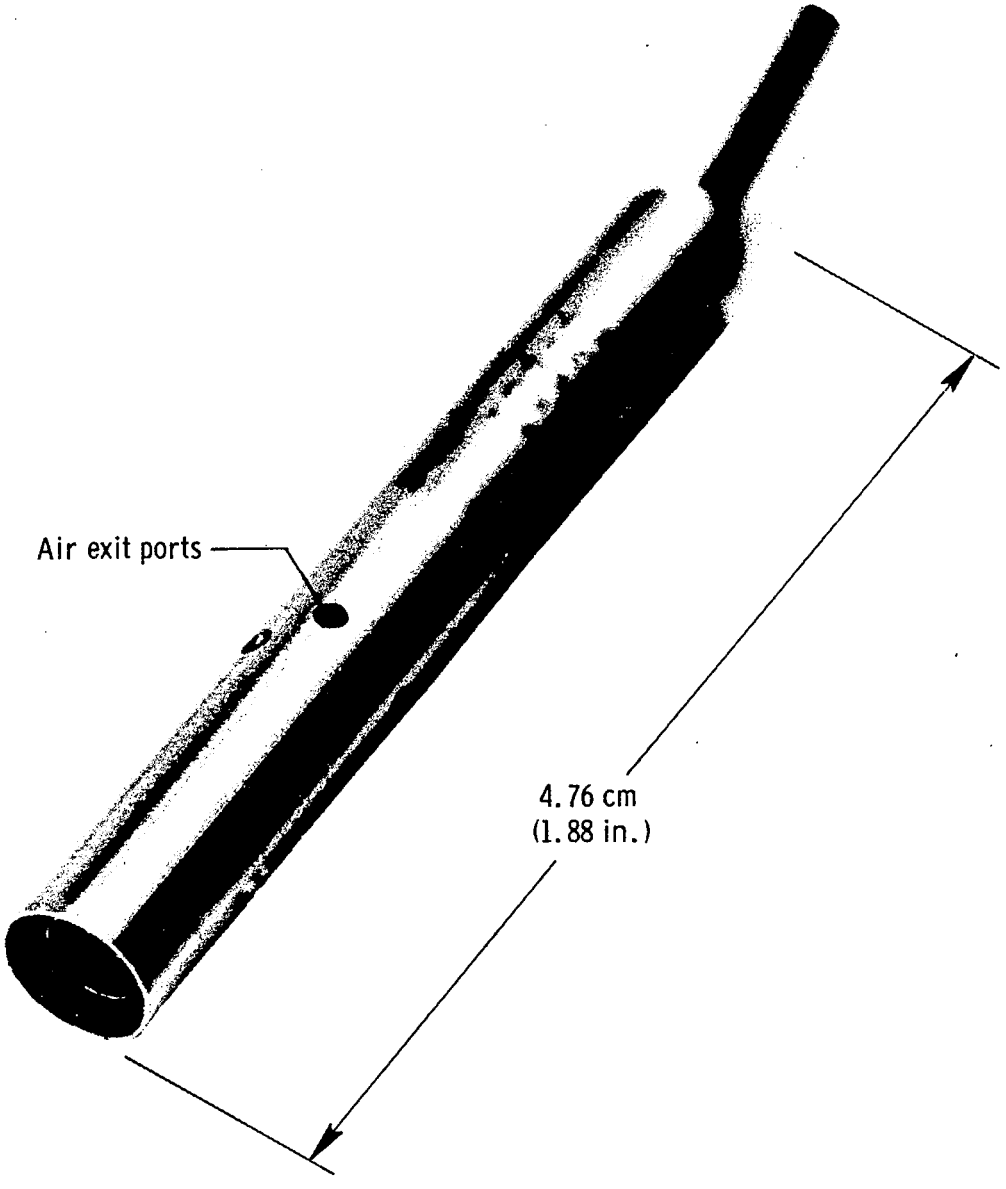

E-18362

(a) Photograph.

Figure 5. Details of the shielded thermocouple probe and recording system.

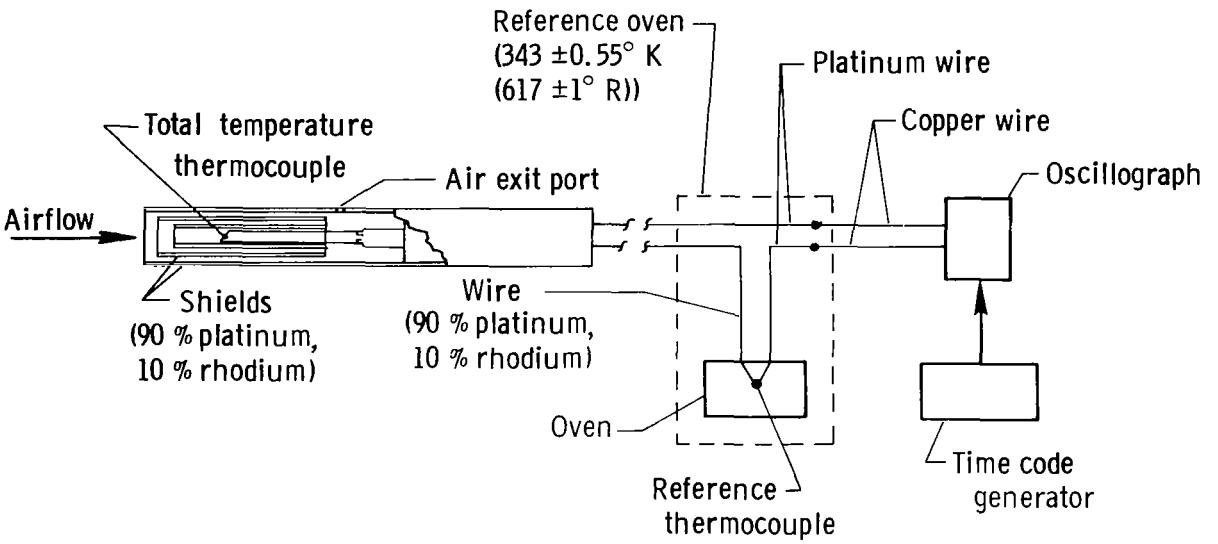

(b) Cutaway drawing and recording system schematic diagram.

Figure 5. Concluded.

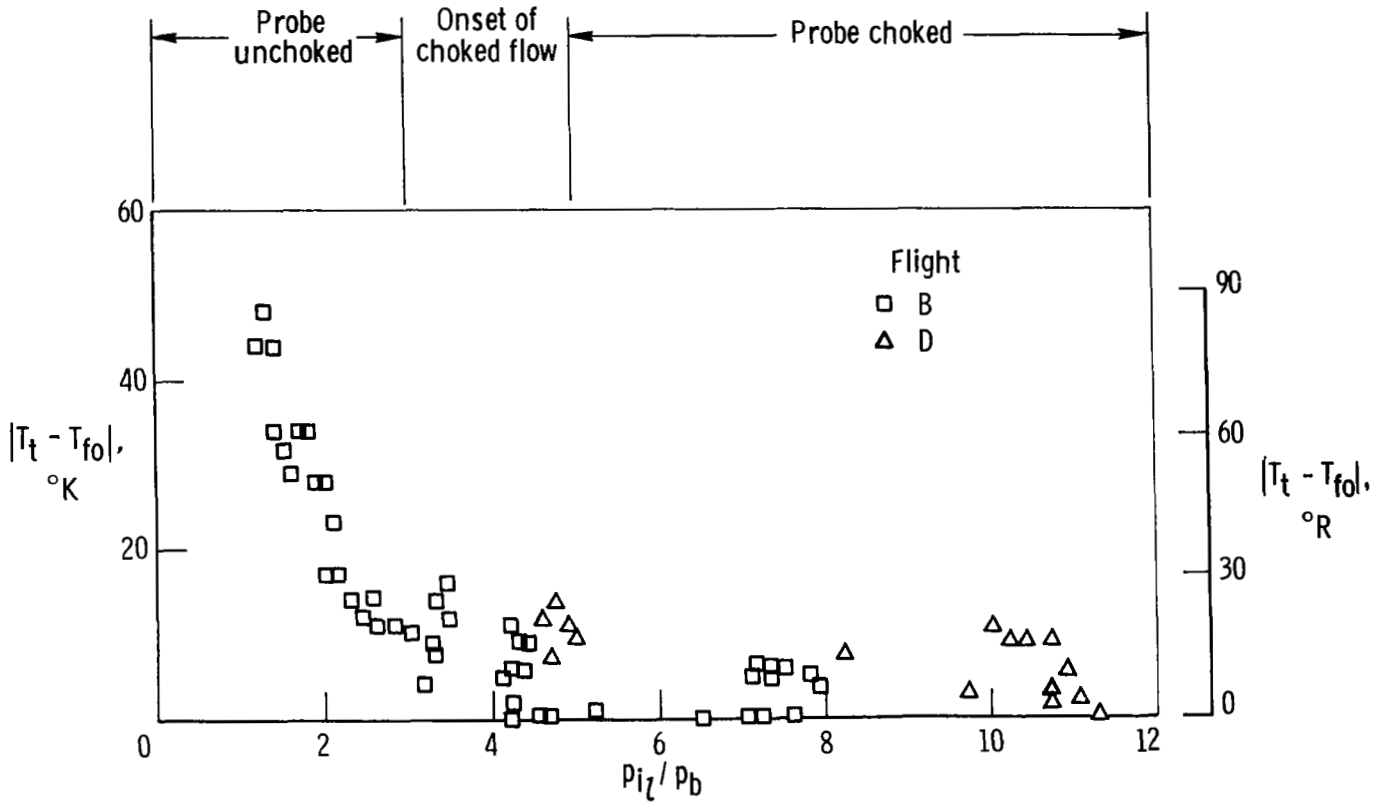

Figure 6. Effect of p_{i_l} / p_b on probe choking and $|T_t - T_{fo}|$ for $\dot{w}_\infty$ greater than approximately 49 kg/m^2-sec (10 lbm/ft^2-sec).

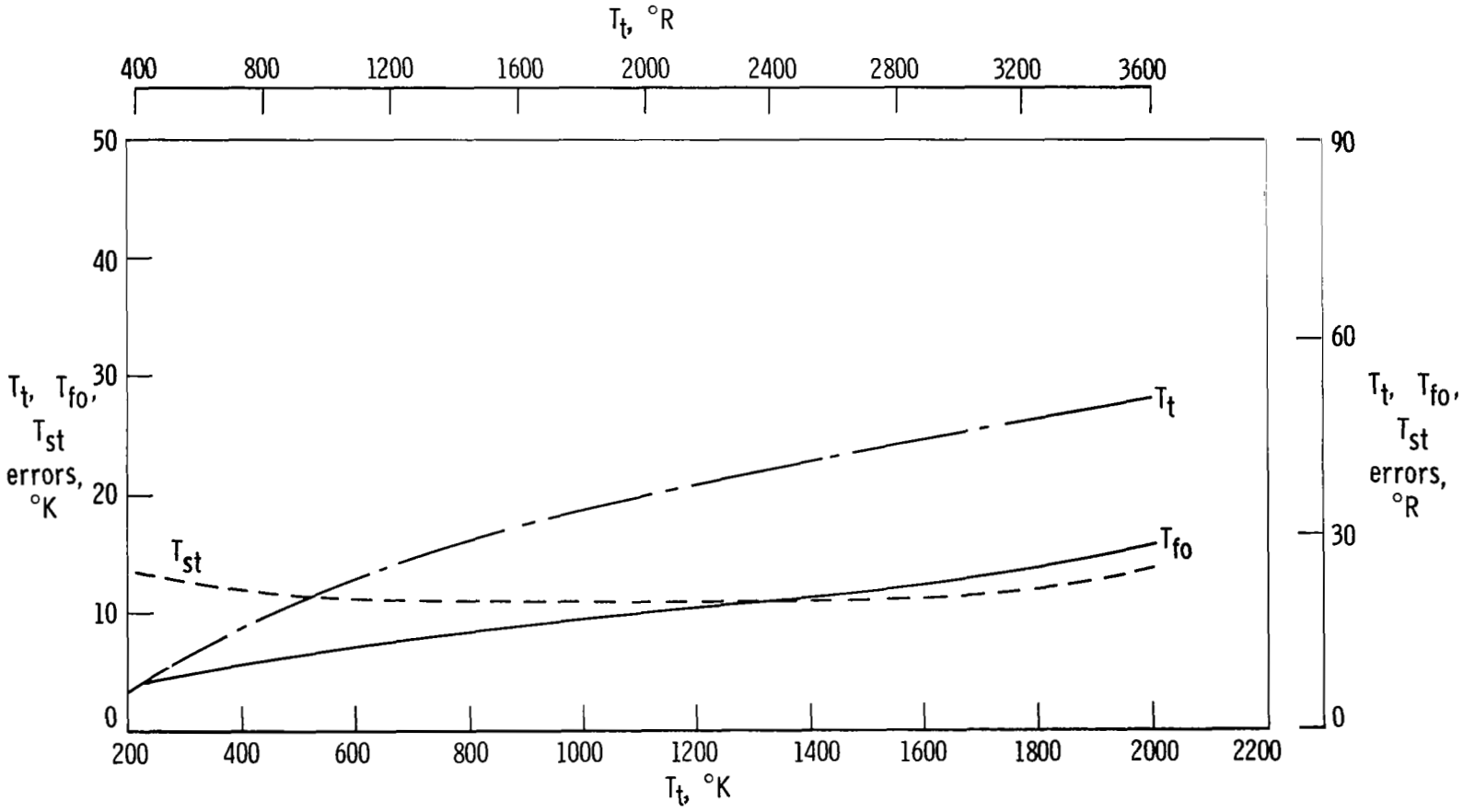

Figure 7. Effect of T_t on temperature measurement and calculation errors.

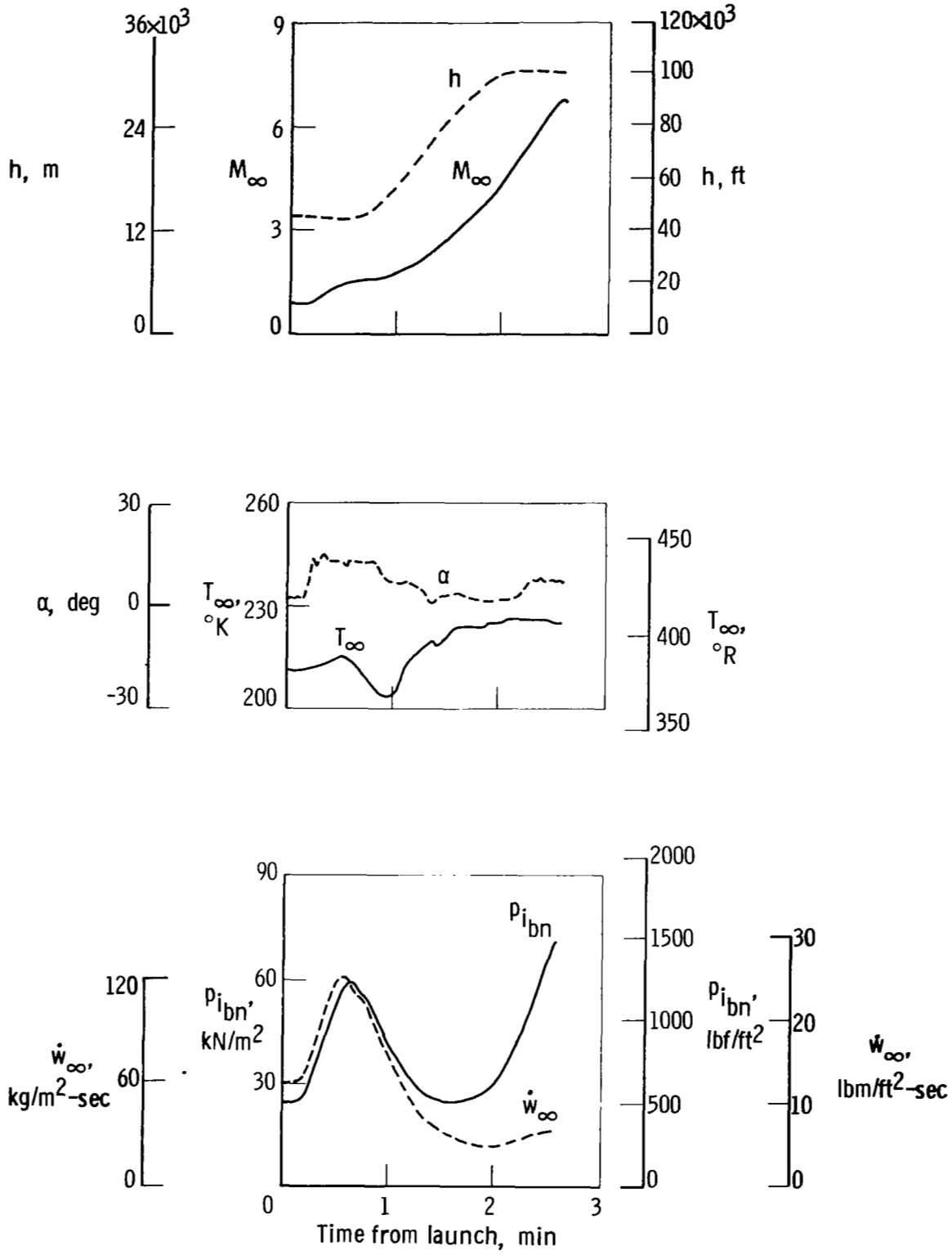

(a) M_∞, h, T_∞, α, $\dot{w}_\infty$, $p_{i_{bn}}$.

Figure 8. Time history of measured and calculated parameters obtained during flight A.

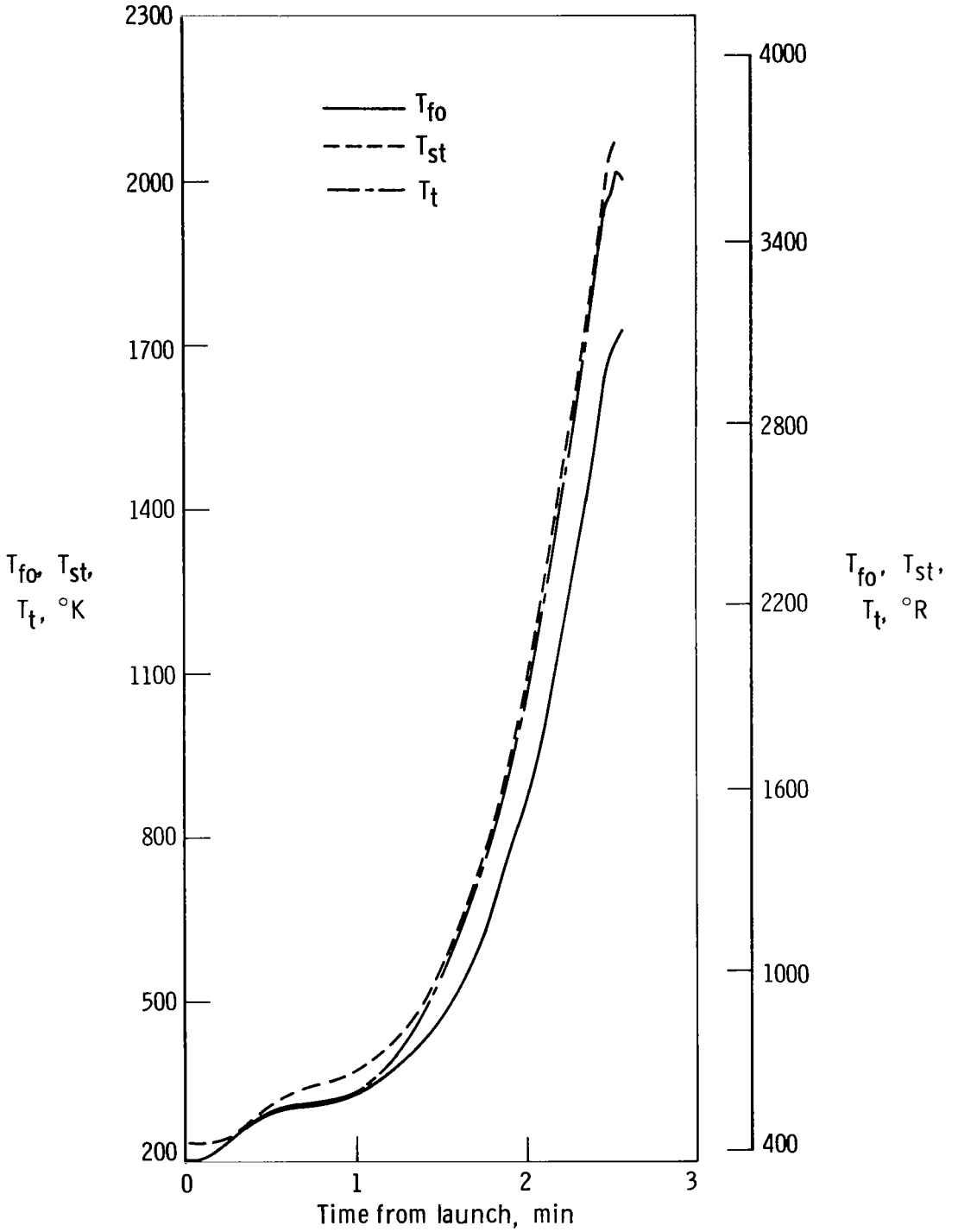

(b) T_{fo}, T_{st}, T_t.

Figure 8. Concluded.

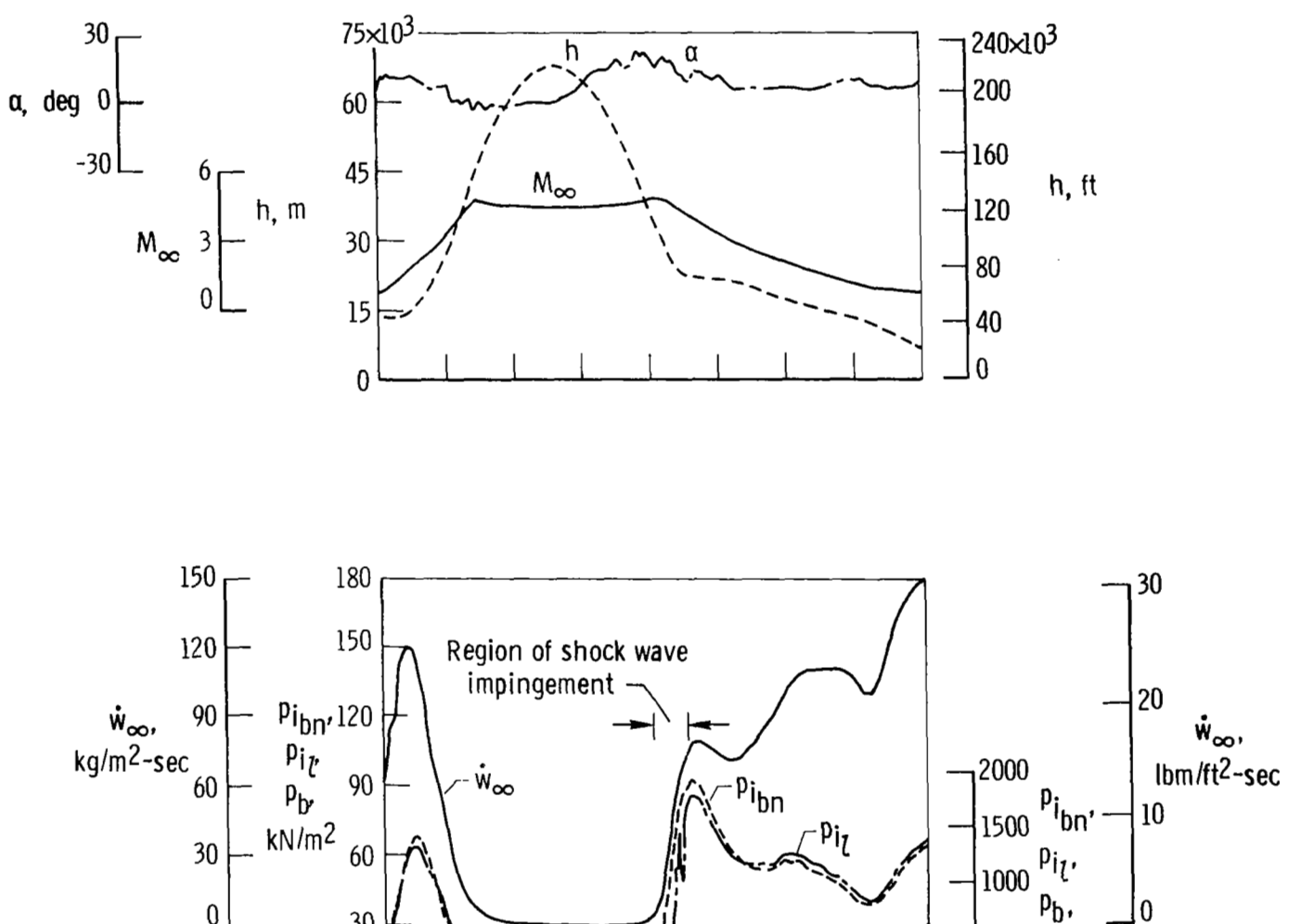

(a) M_∞, h, α, $p_{i_{bn}}$, p_{i_ℓ}, p_b, $\dot{w}_\infty$.

Figure 9. Time history of measured and calculated parameters obtained during flight B.

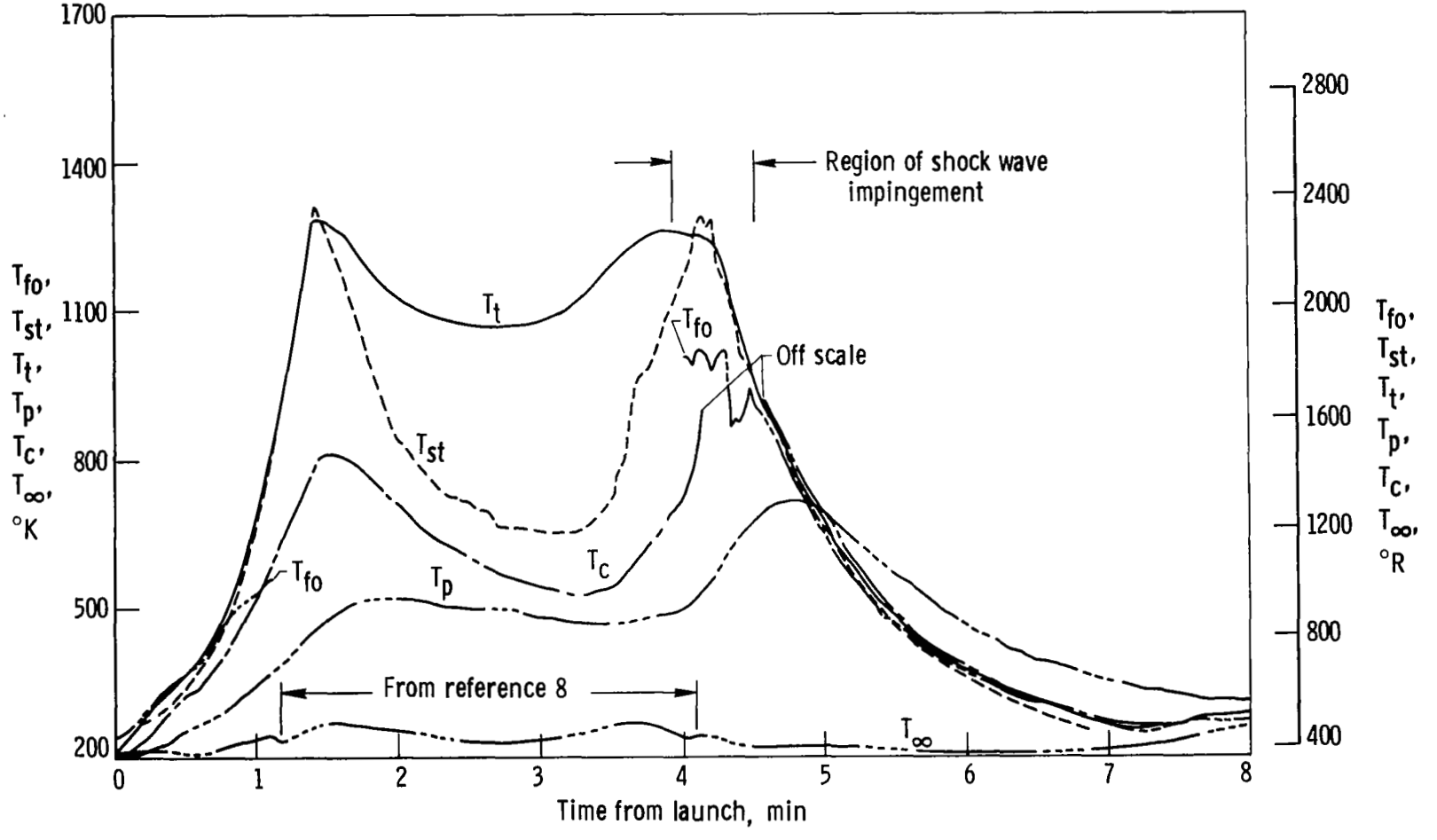

(b) T_{fo}, T_{st}, T_t, T_p, T_c, T_∞.

Figure 9. Concluded.

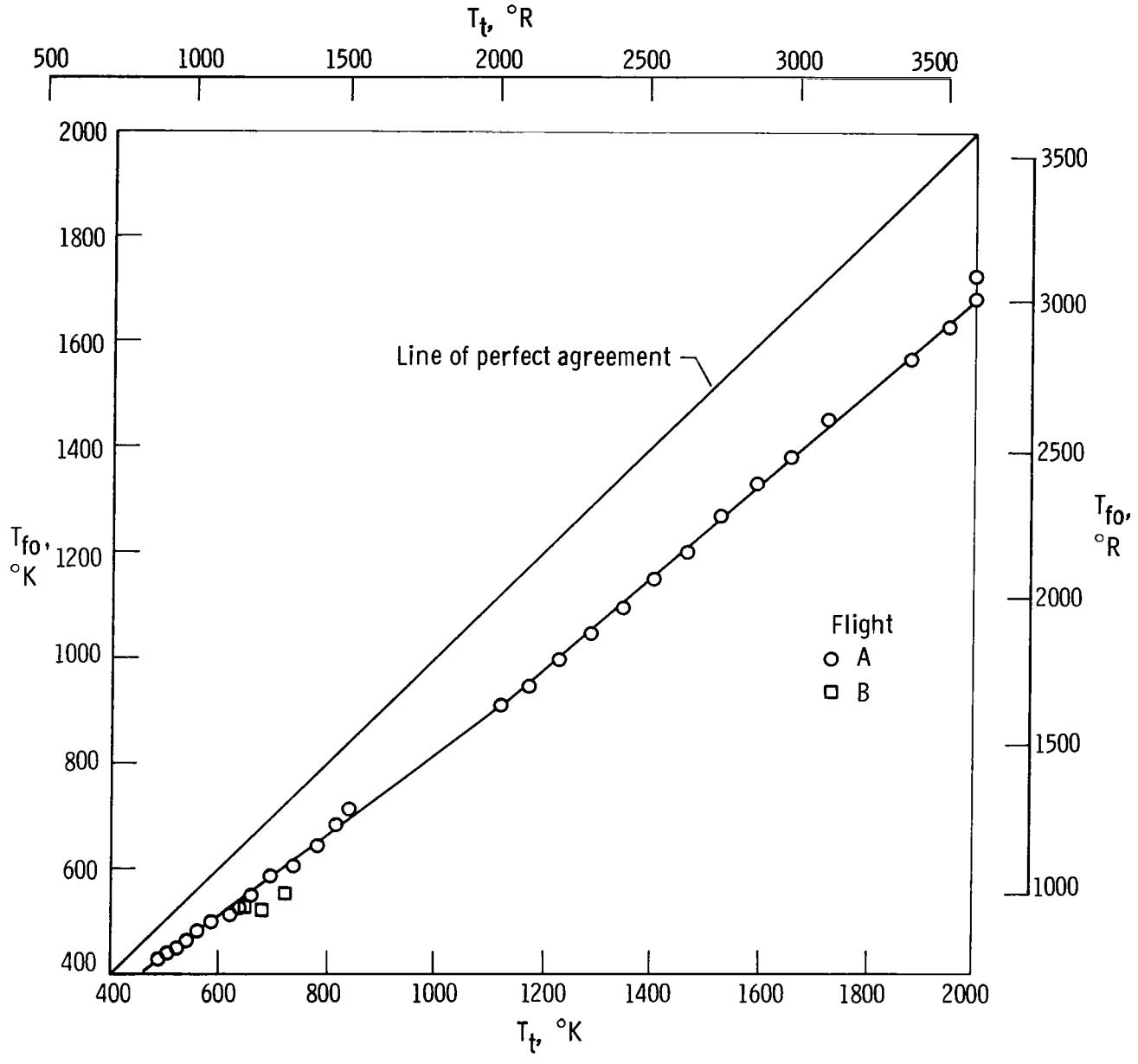

(a) $\dot{w}_\infty = 30 \pm 6$ kg/m^2-sec (6.1 ±1.2 lbm/ft^2-sec).

Figure 10. Variation of T_{fo} with T_t for approximately constant values of $\dot{w}_\infty$.

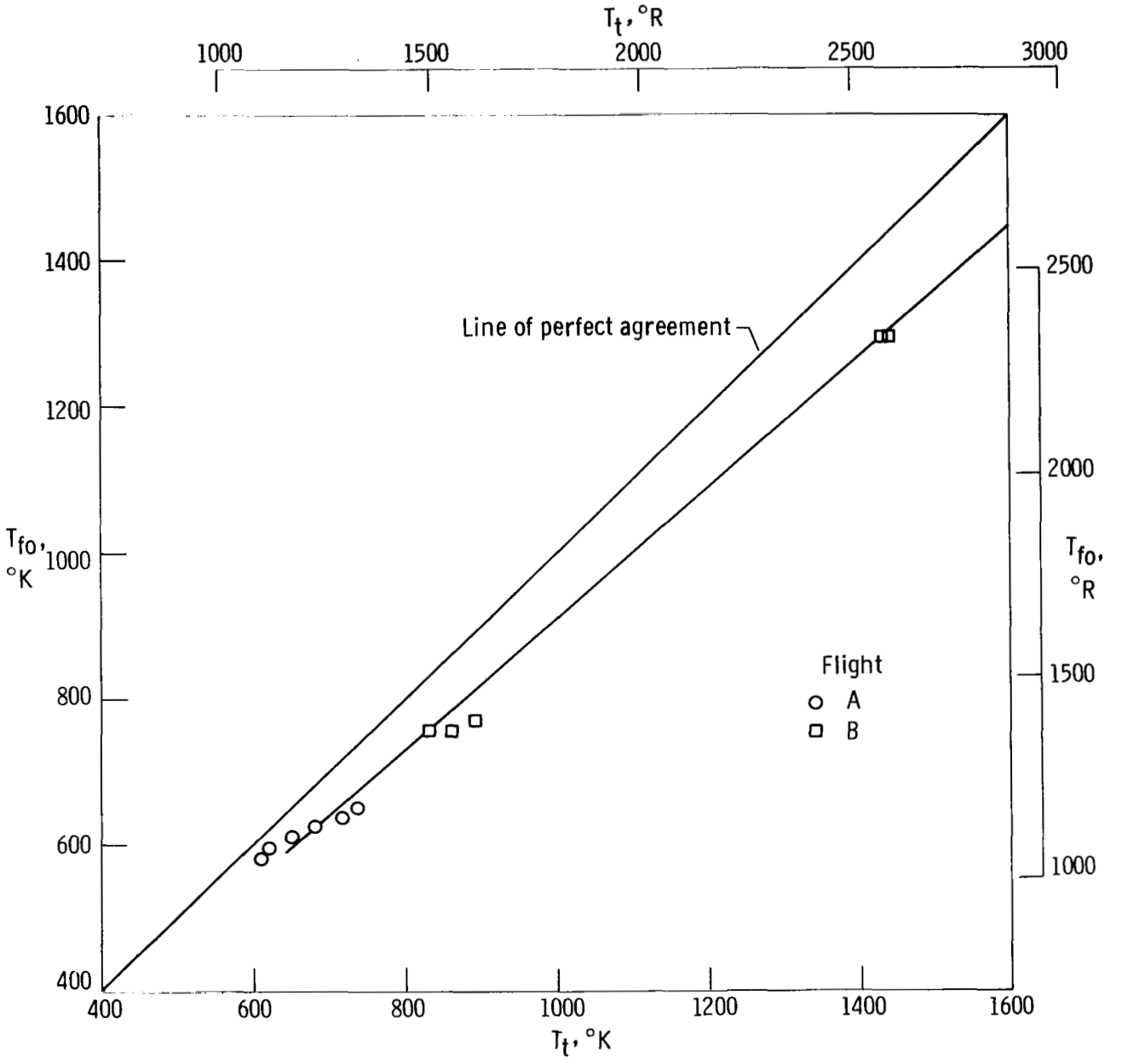

(b) $\dot{w}_\infty$ = 42 ±6 kg/m^2-sec (8.6 ±1.2 lbm/ft^2-sec).

Figure 10. Continued.

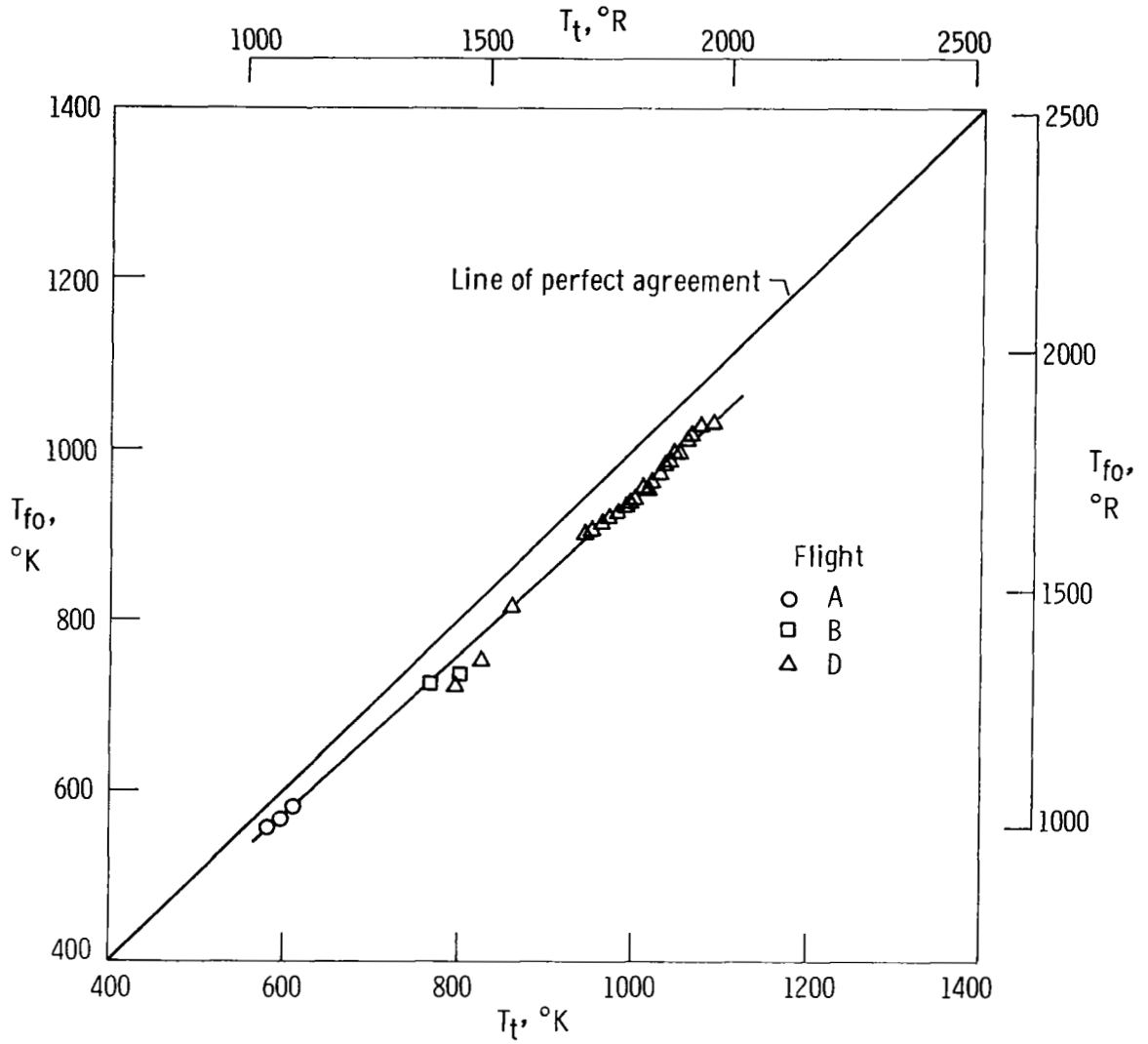

(c) $\dot{w}_\infty$ = 54 ±6 kg/m^2-sec (11.0 ±1.2 lbm/ft^2-sec).

Figure 10. Continued.

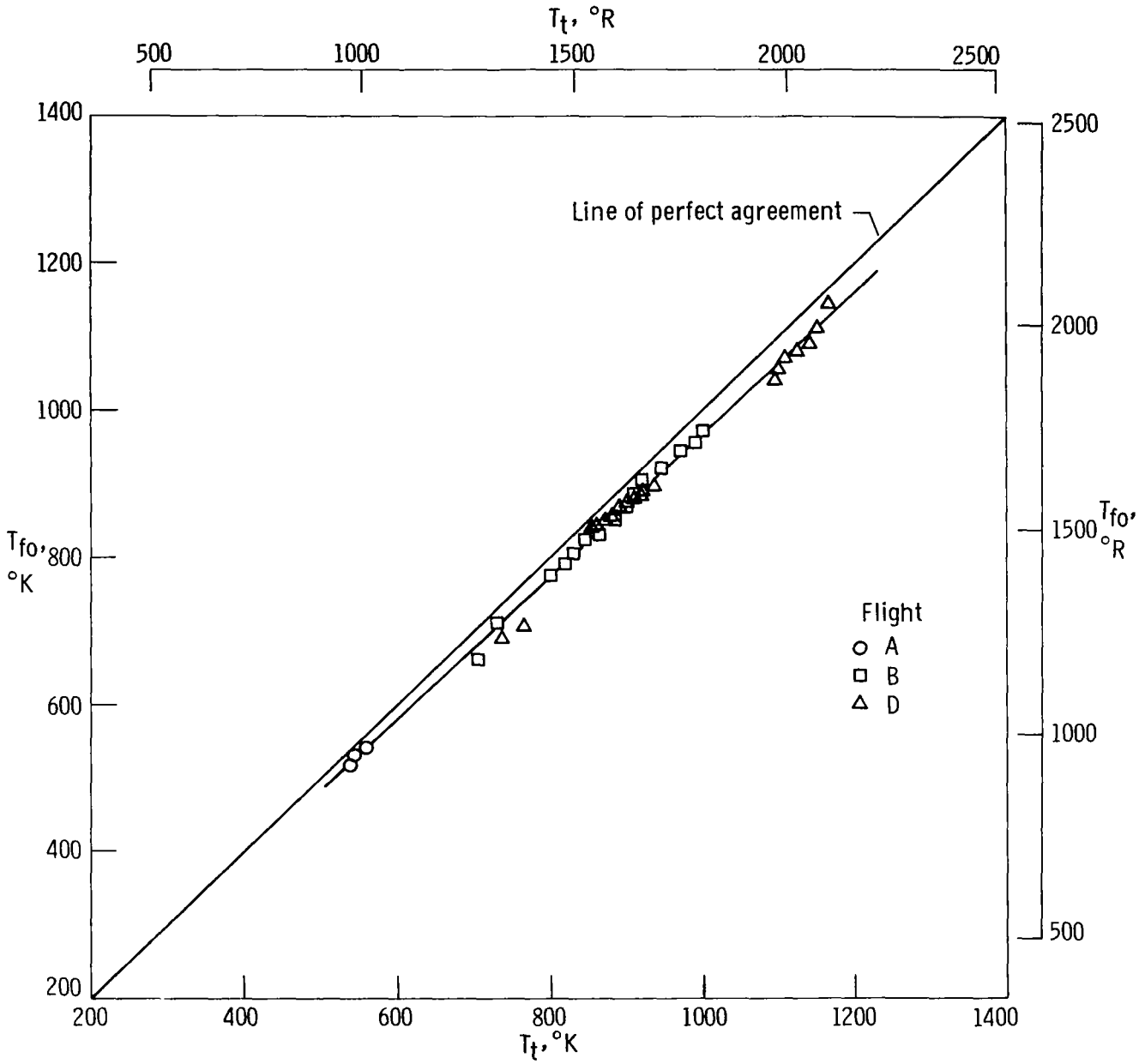

(d) $\dot{w}_\infty$ = 66 ±6 kg/m^2-sec (13.5 ±1.2 lbm/ft^2-sec).

Figure 10. Continued.

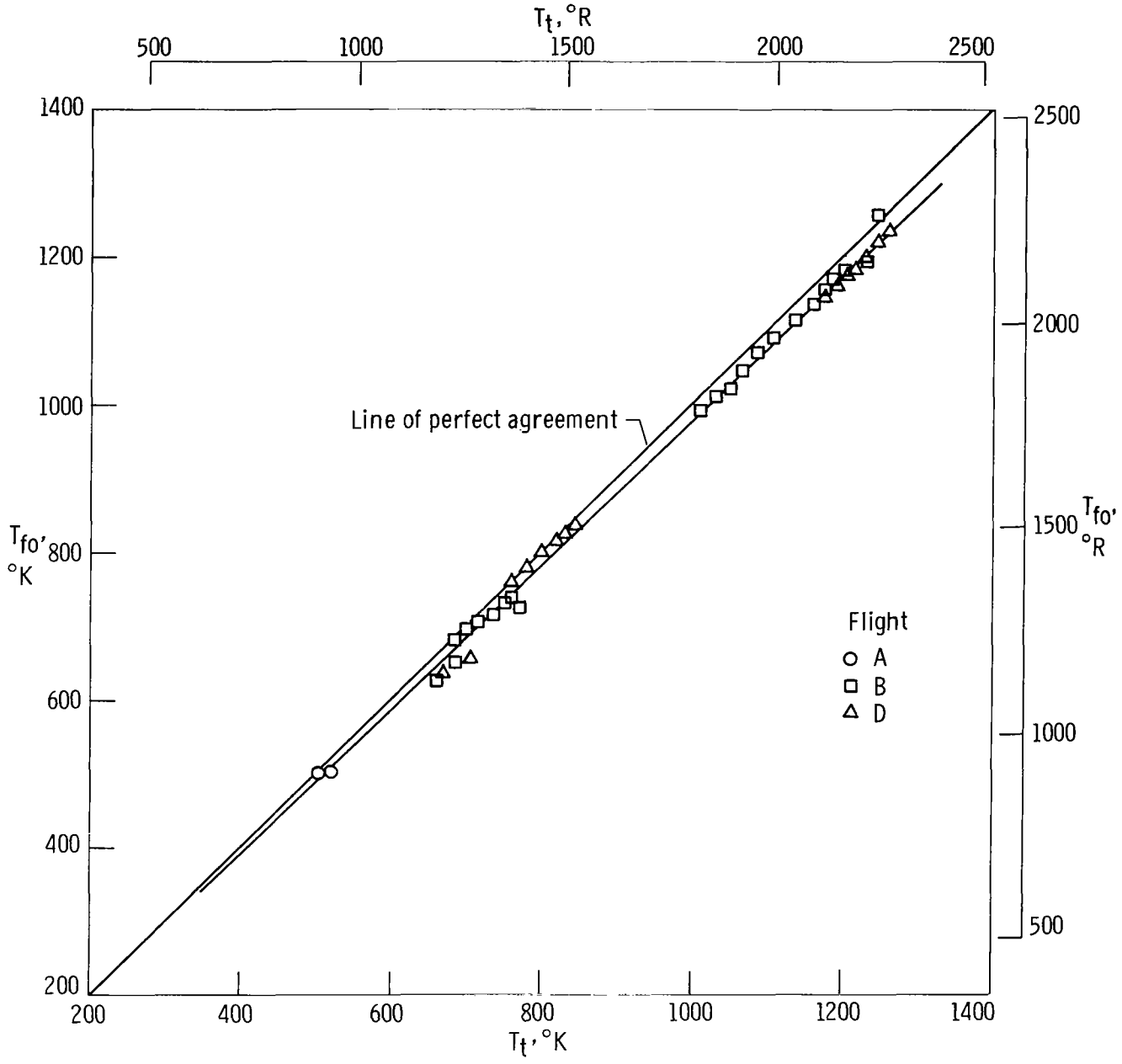

(e) $\dot{w}_\infty = 78 \pm 6$ kg/m^2-sec (16.0 ±1.2 lbm/ft^2-sec).

Figure 10. Continued.

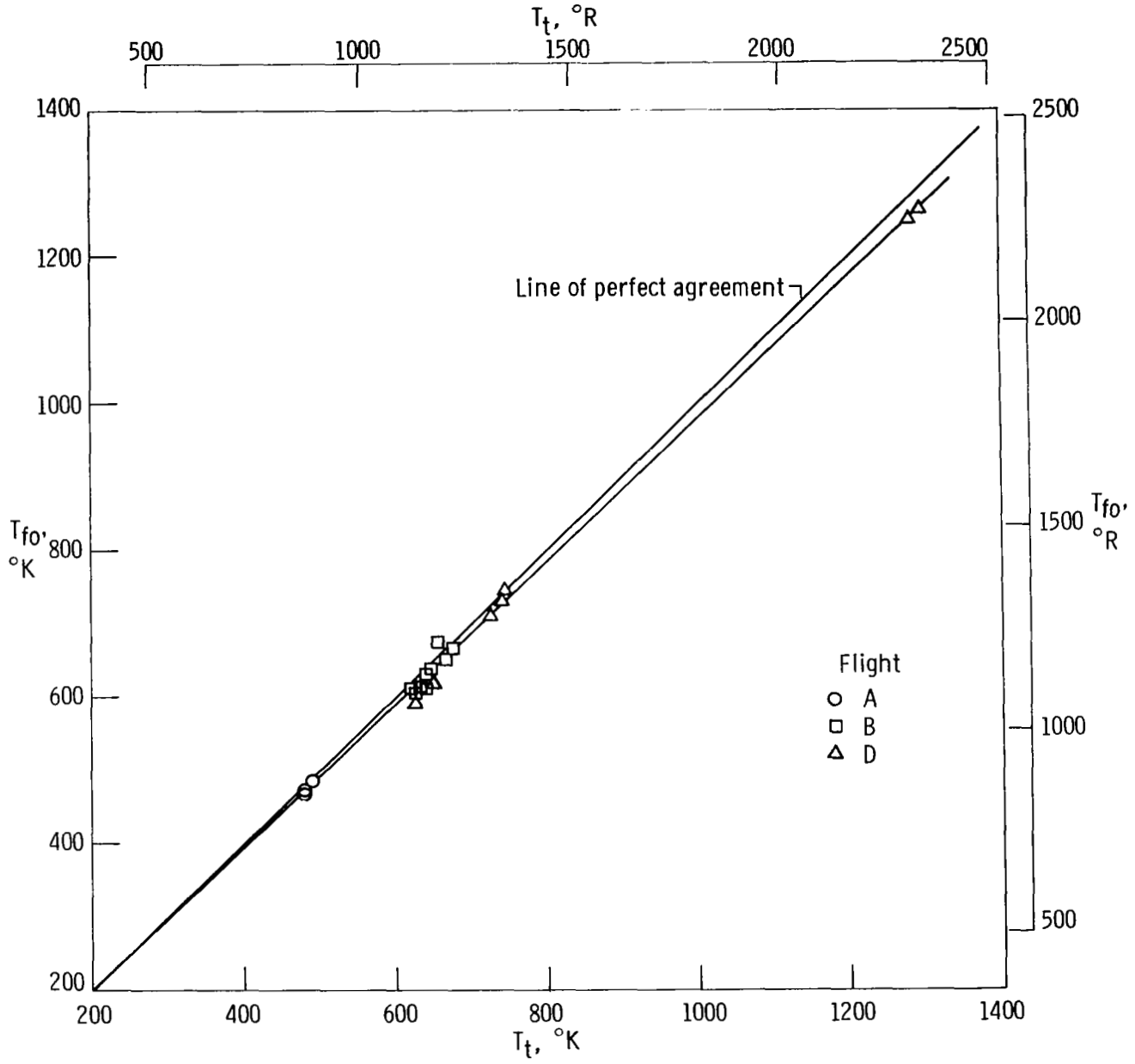

(f) $\dot{w}_\infty = 90 \pm 6$ kg/m^2-sec (18.4 ± 1.2 lbm/ft^2-sec).

Figure 10. Continued.

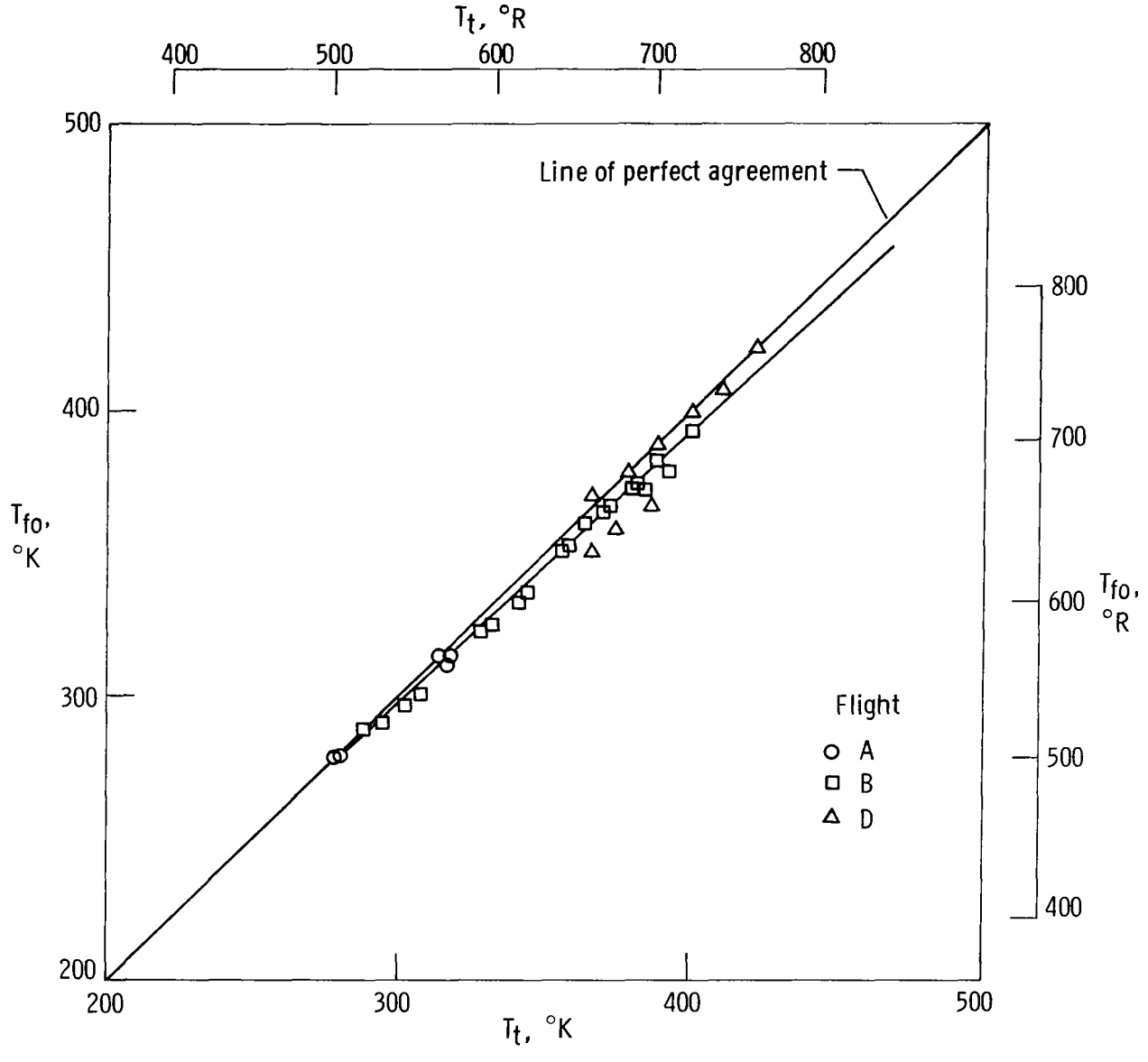

(g) $\dot{w}_\infty$ = 102 ±6 kg/m^2-sec (20.9 ±1.2 lbm/ft^2-sec).

Figure 10. Continued.

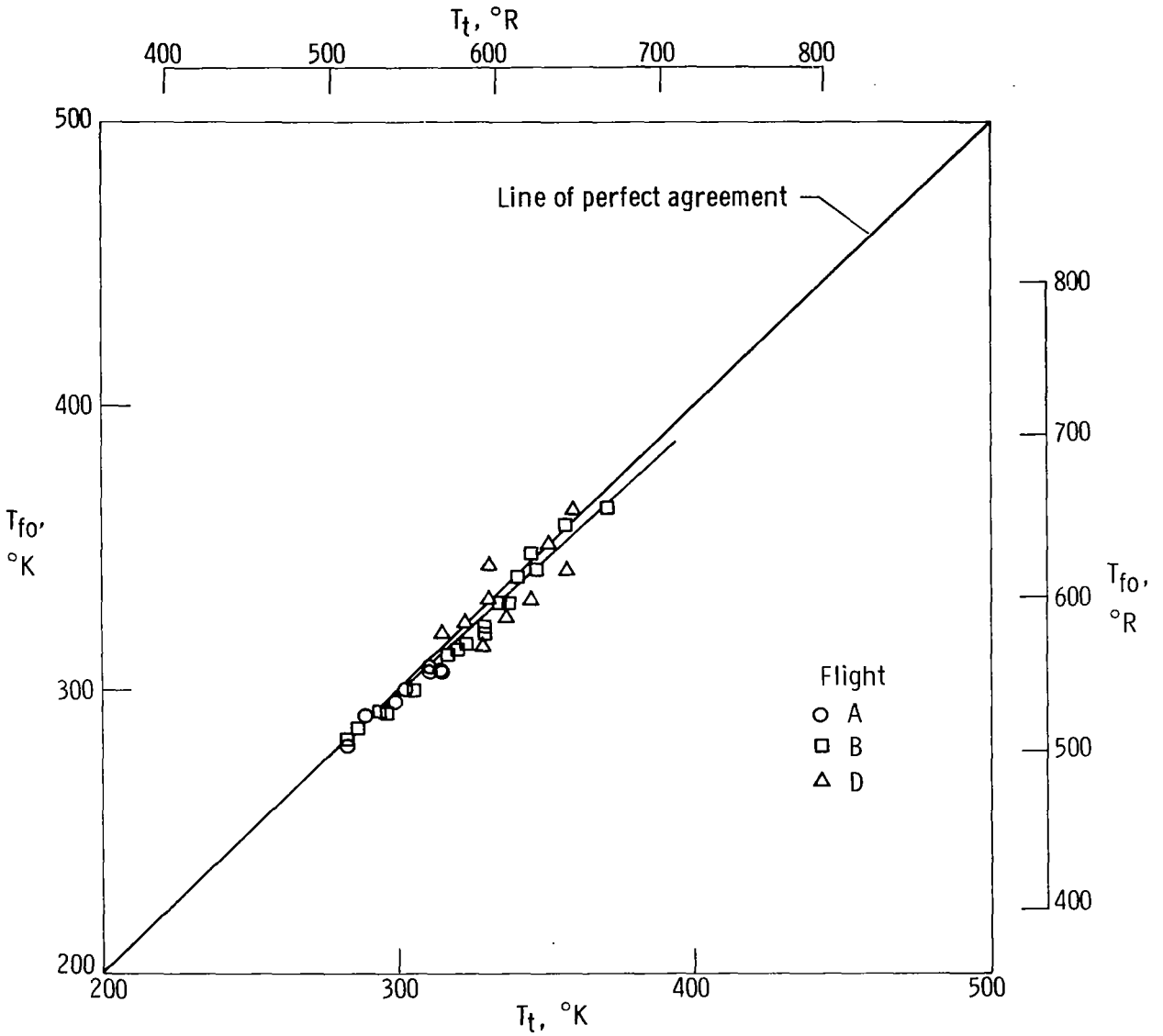

(h) $\dot{w}_\infty = 114 \pm 6$ kg/m^2-sec (23.4 ±1.2 lbm/ft^2-sec).

Figure 10. Concluded.

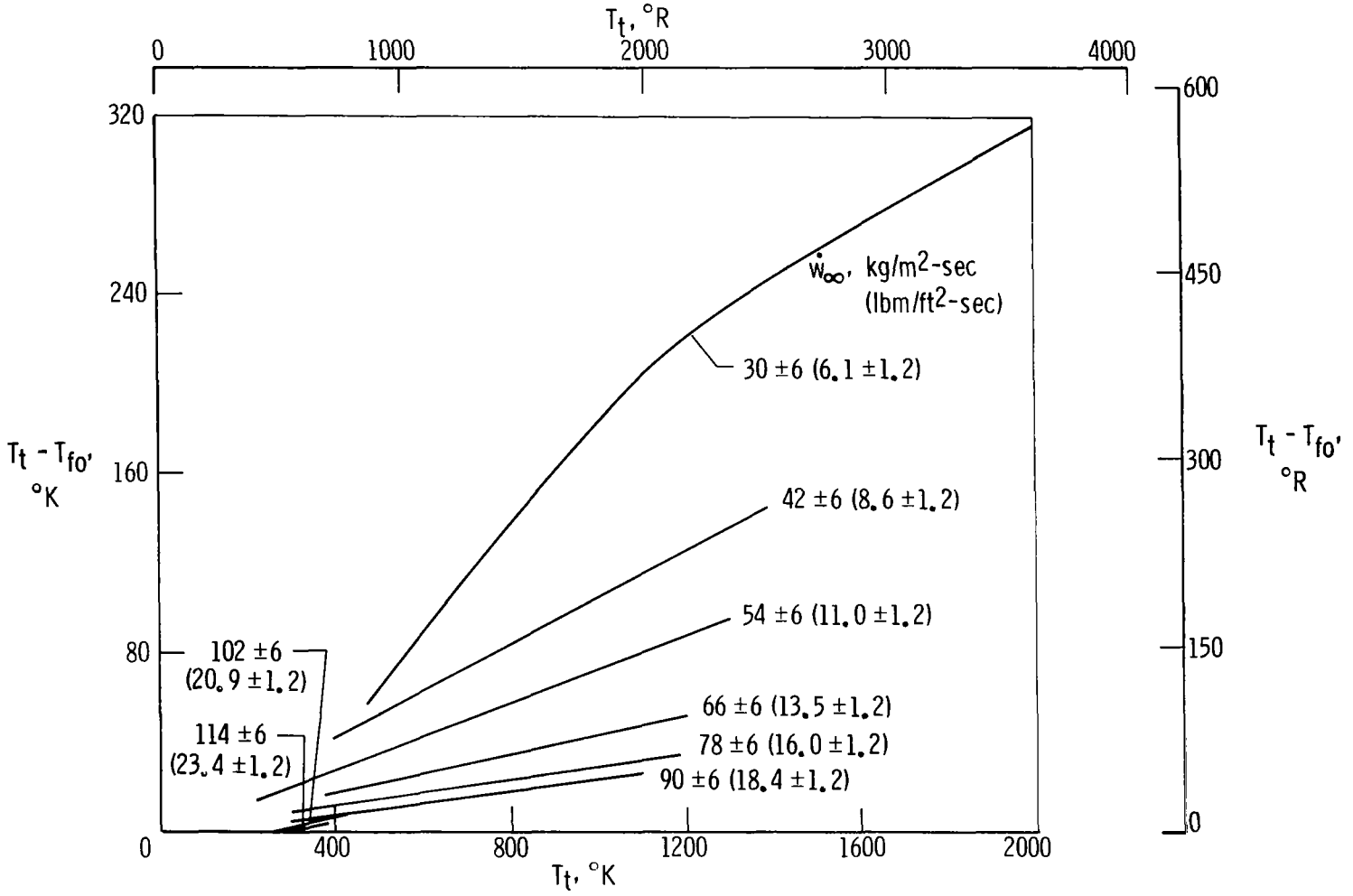

Figure 11. Effect of T_t on $T_t - T_{fo}$ for approximately constant values of $\dot{w}_\infty$.

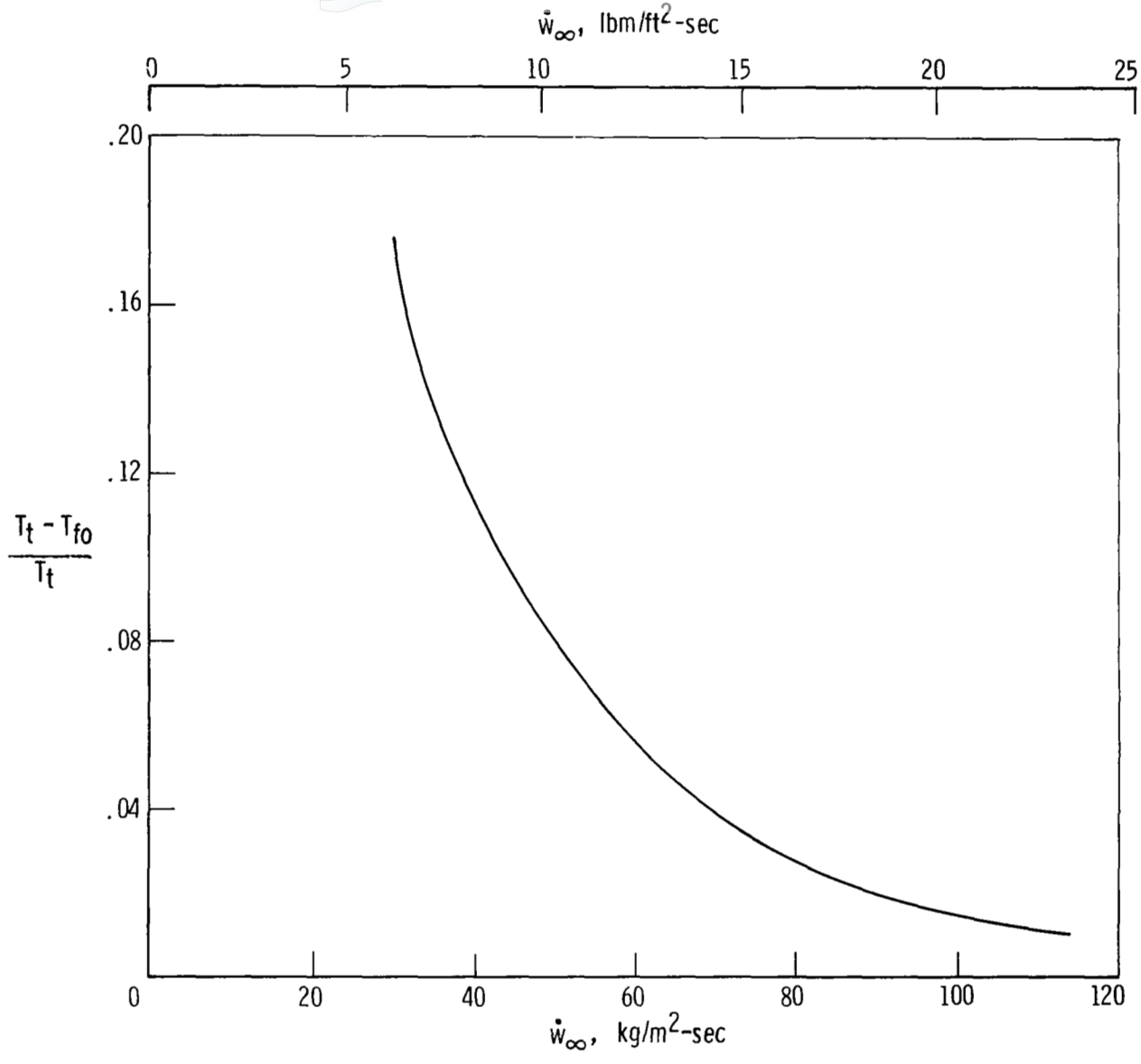

Figure 12. Variation of $\frac{T_t - T_{fo}}{T_t}$ with $\dot{w}_\infty$ for fluidic oscillator probe.

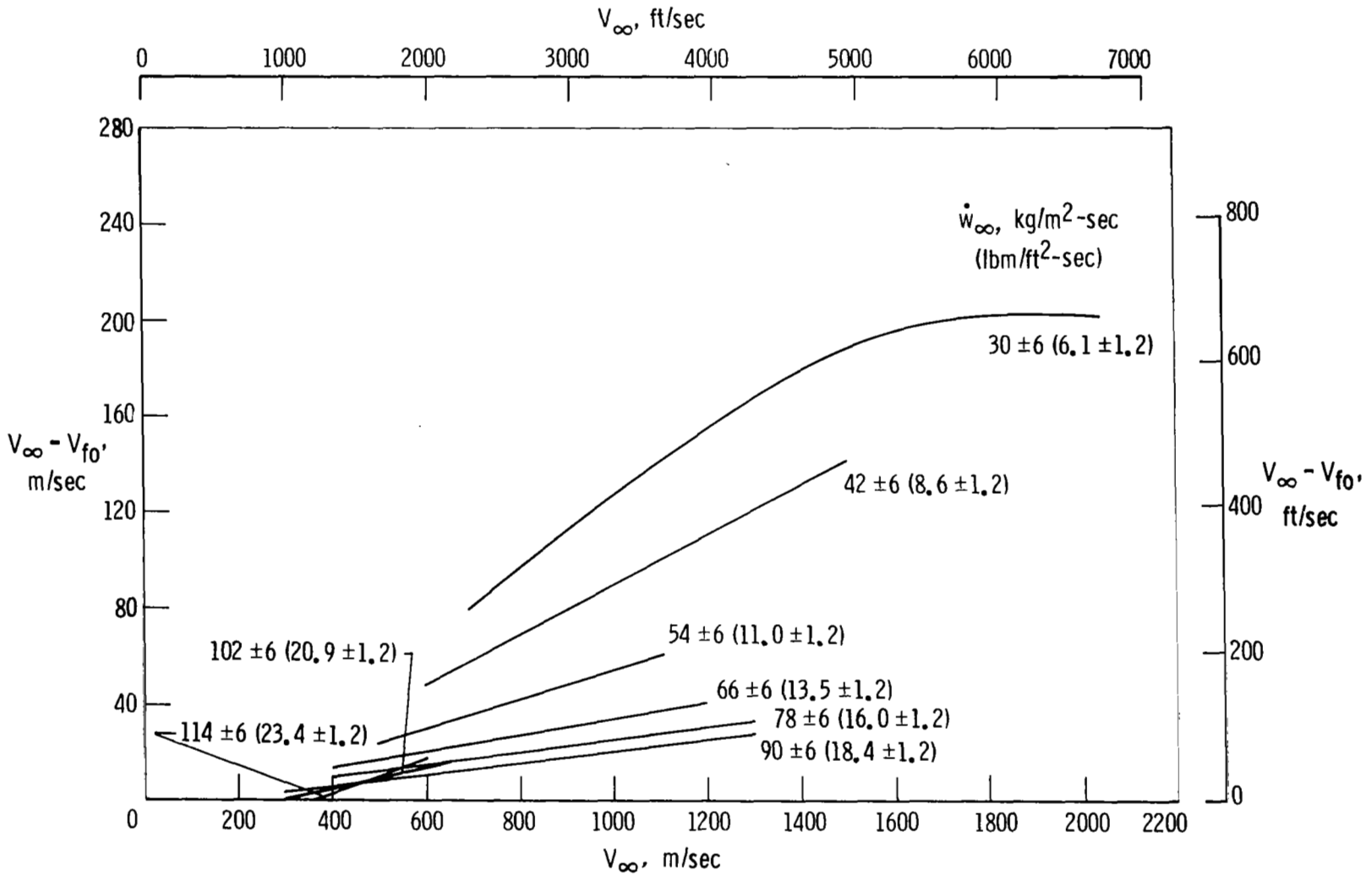

Figure 13. Effect of V_∞ on $V_\infty - V_{fo}$ for approximately constant values of $\dot{w}_\infty$.

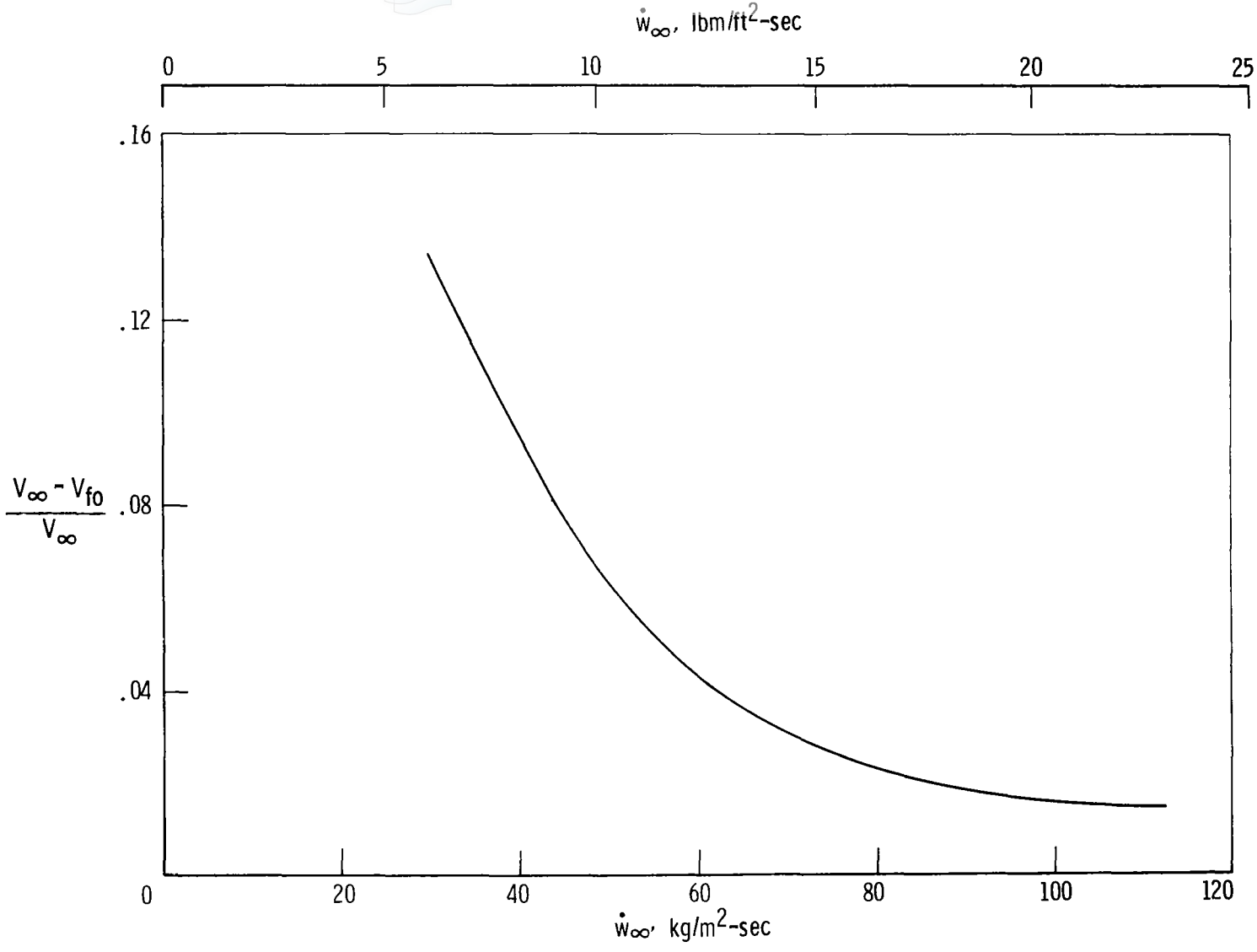

Figure 14. Variation of $\frac{V_\infty - V_{fo}}{V_\infty}$ with $\dot{w}_\infty$ for fluidic oscillator probe.

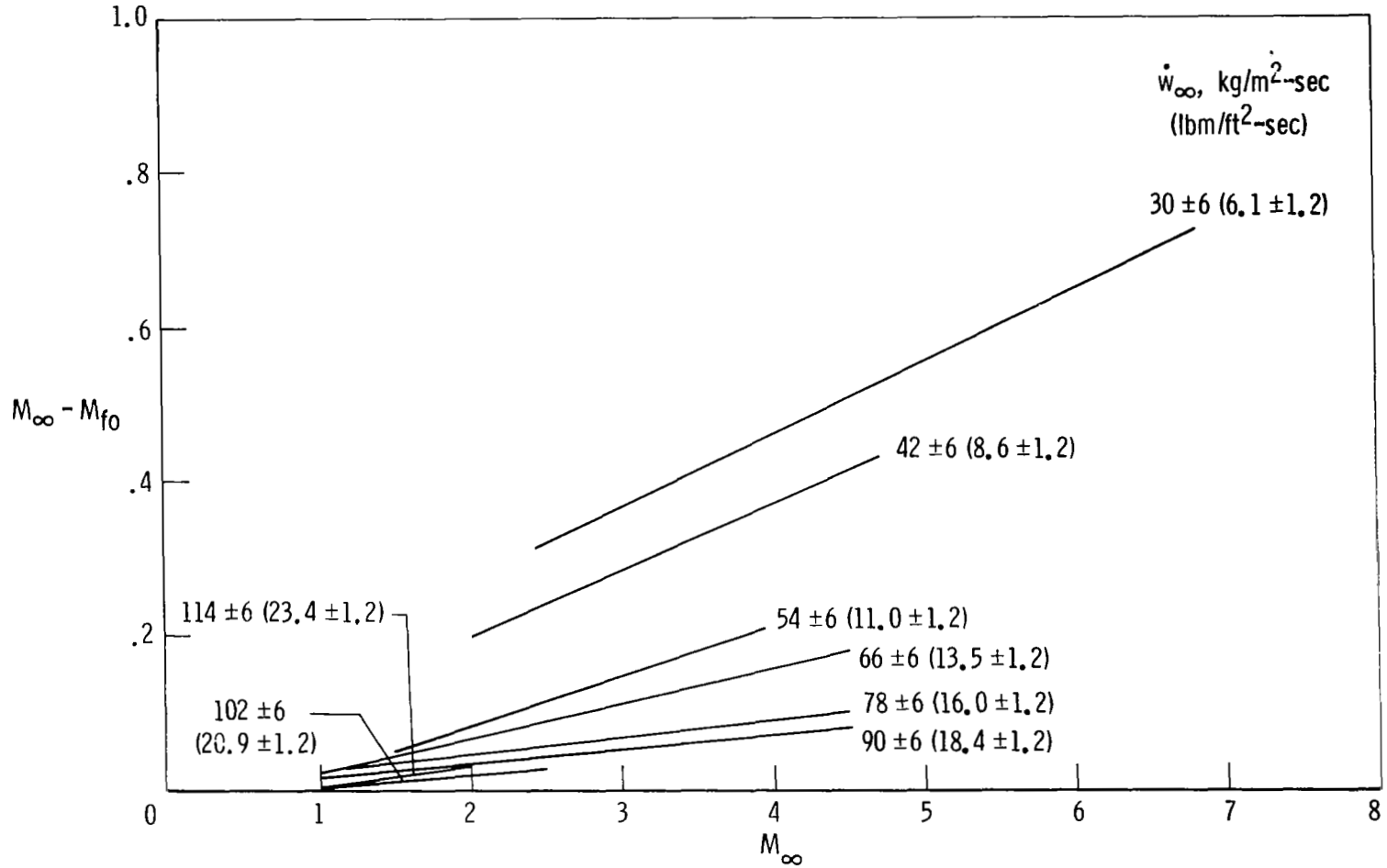

Figure 15. Effect of M_∞ on $M_\infty - M_{f0}$ for approximately constant values of $\dot{w}_\infty$.

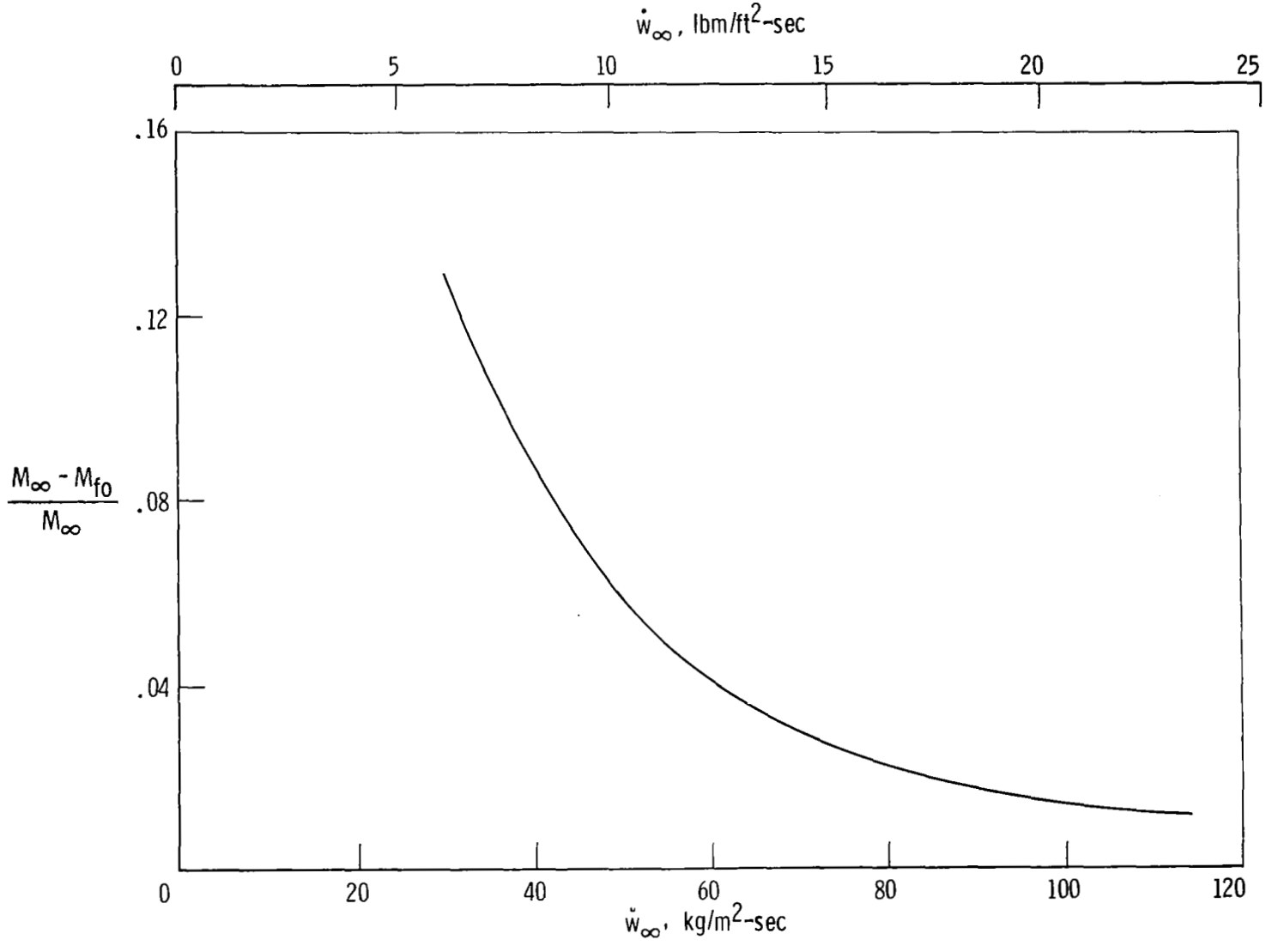

Figure 16. Variation of $\frac{M_\infty - M_{fo}}{M_\infty}$ with $\dot{w}_\infty$ for fluidic oscillator probe.

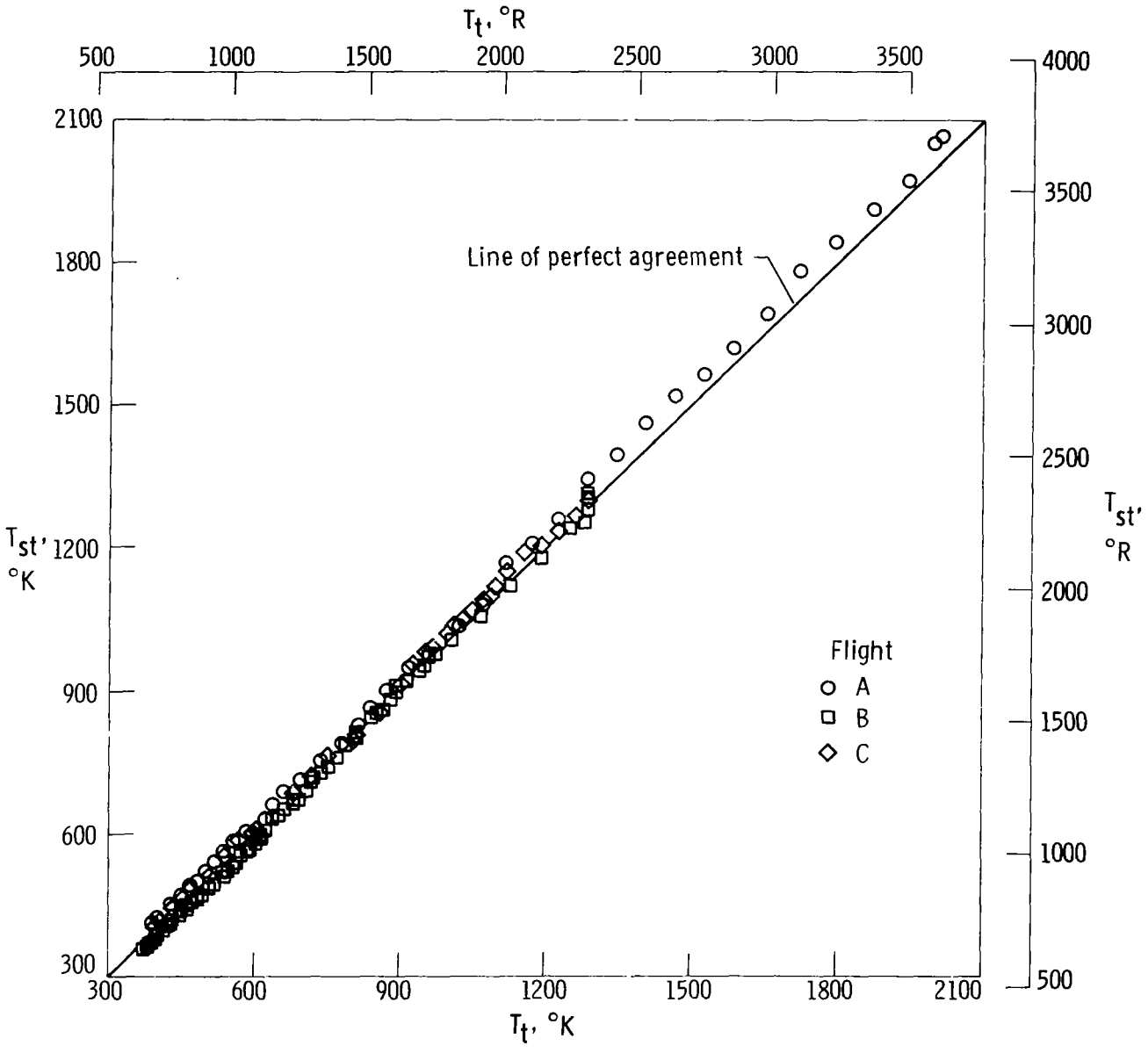

Figure 17. Variation of T_{st} with T_t for shielded thermocouple probe. $M_\infty > 2.0$; $p_{i_l} > 9.6$ kN/m^2 (200 lbf/ft^2).

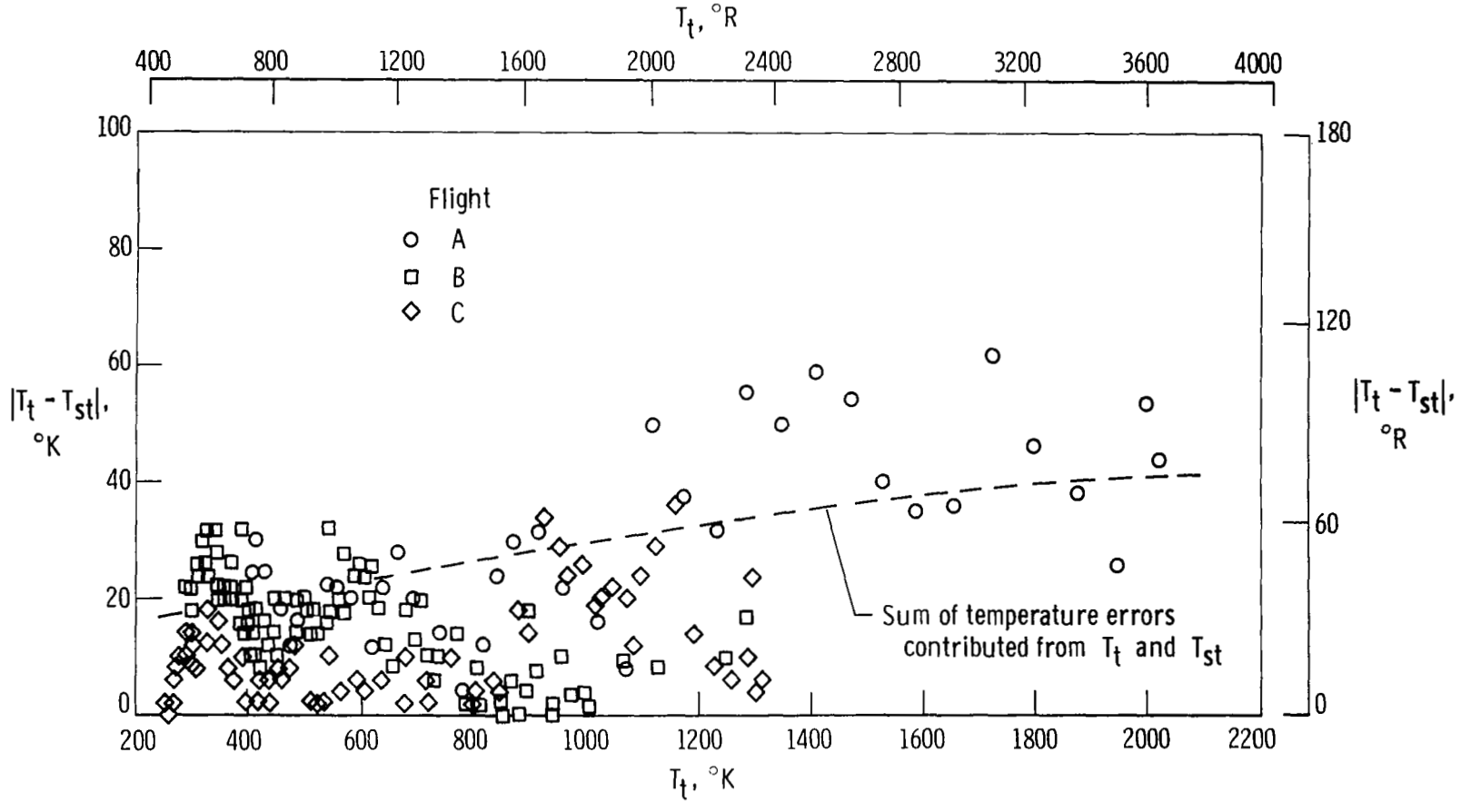

Figure 18. Absolute values of the temperature difference between T_t and T_{st} for a range of T_t.

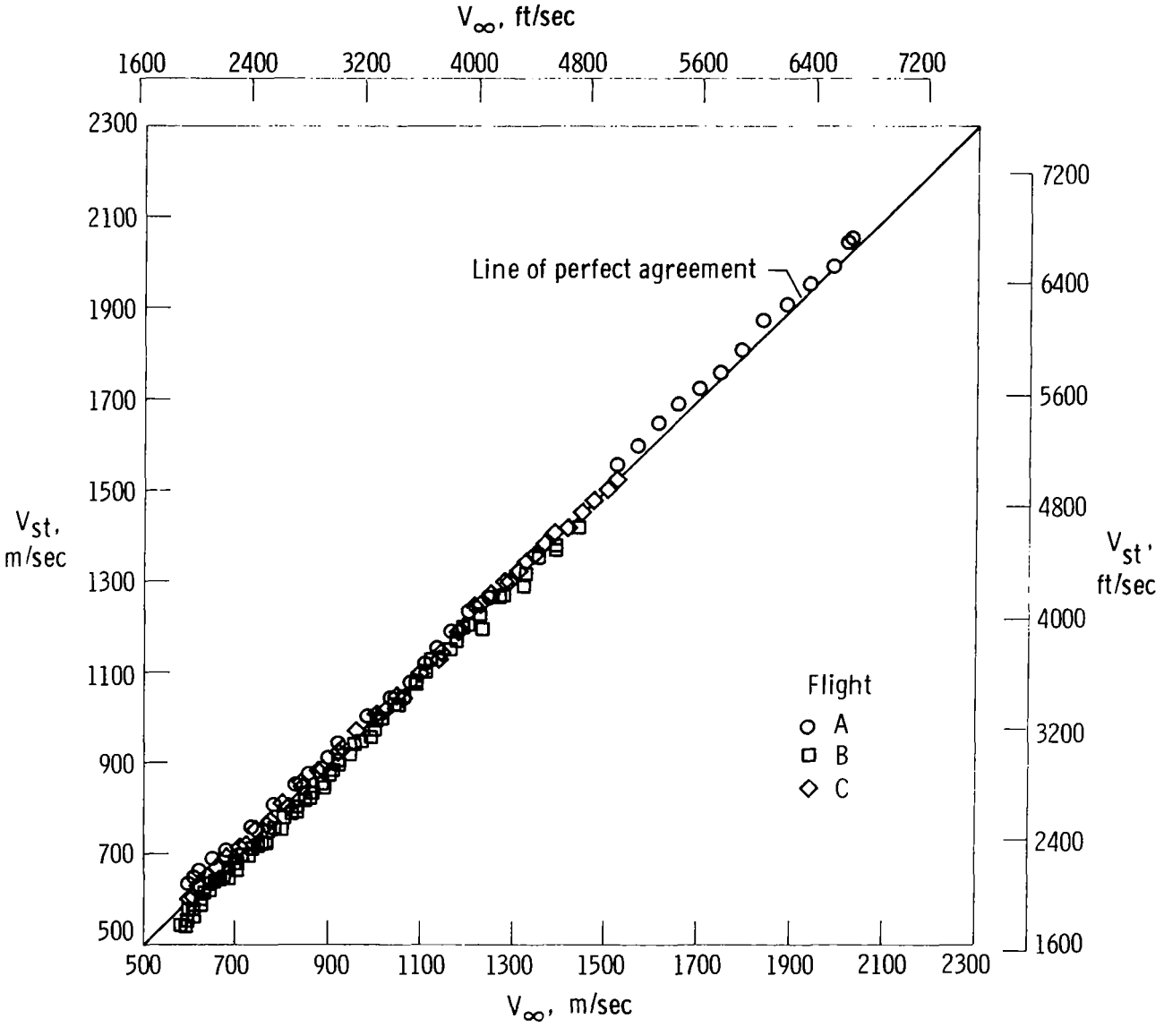

Figure 19. Variation of V_{st} with V_∞ for shielded thermocouple probe, $M_\infty > 2.0$; $p_{i_l} > 9.6$ kN/m^2 (200 lbf/ft^2).

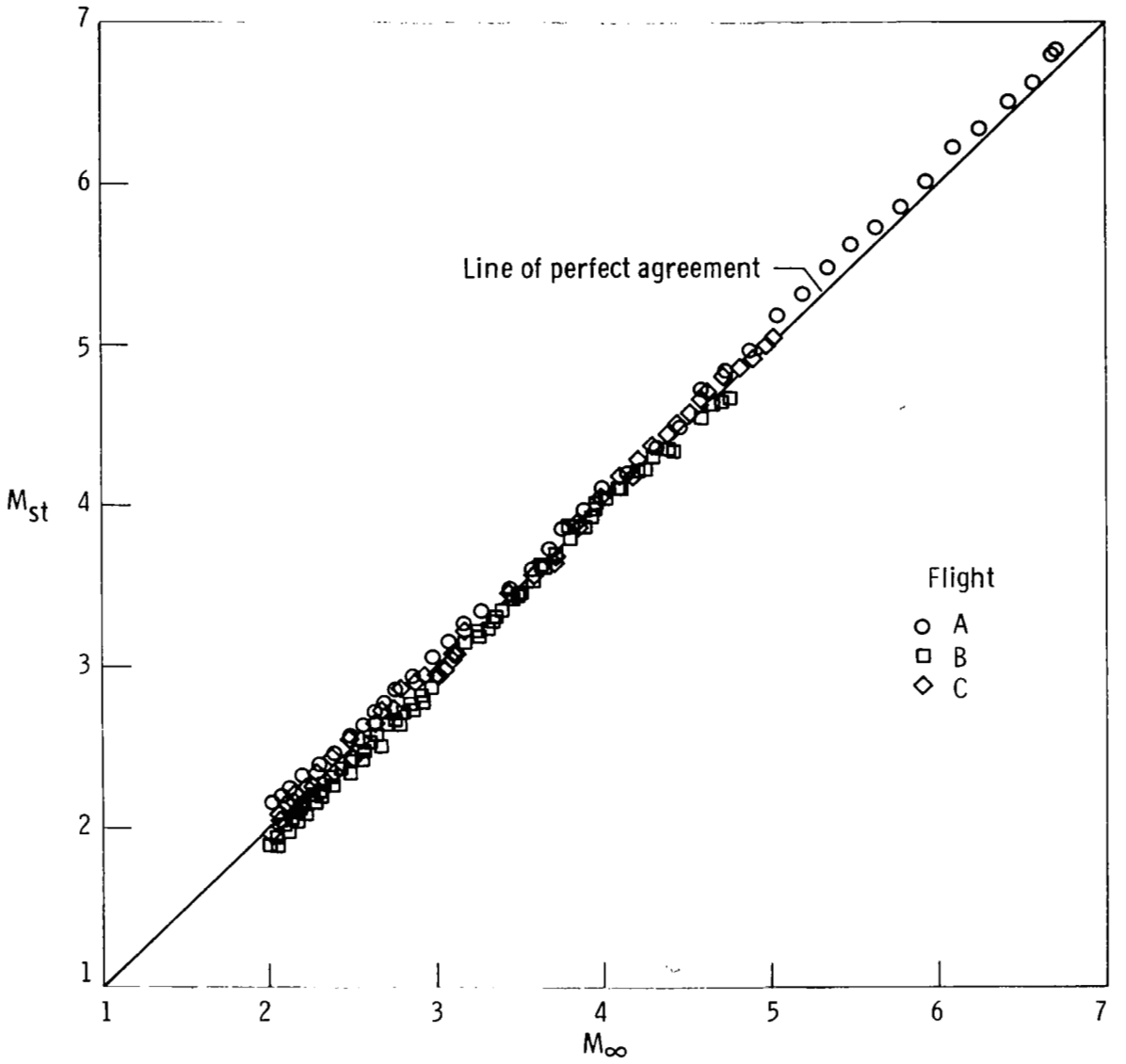

Figure 20. Variation of M_{st} with M_∞ for shielded thermocouple probe. $M_\infty > 2.0$; $p_{i_l} > 9.6$ kN/m^2 (200 lbf/ft^2).

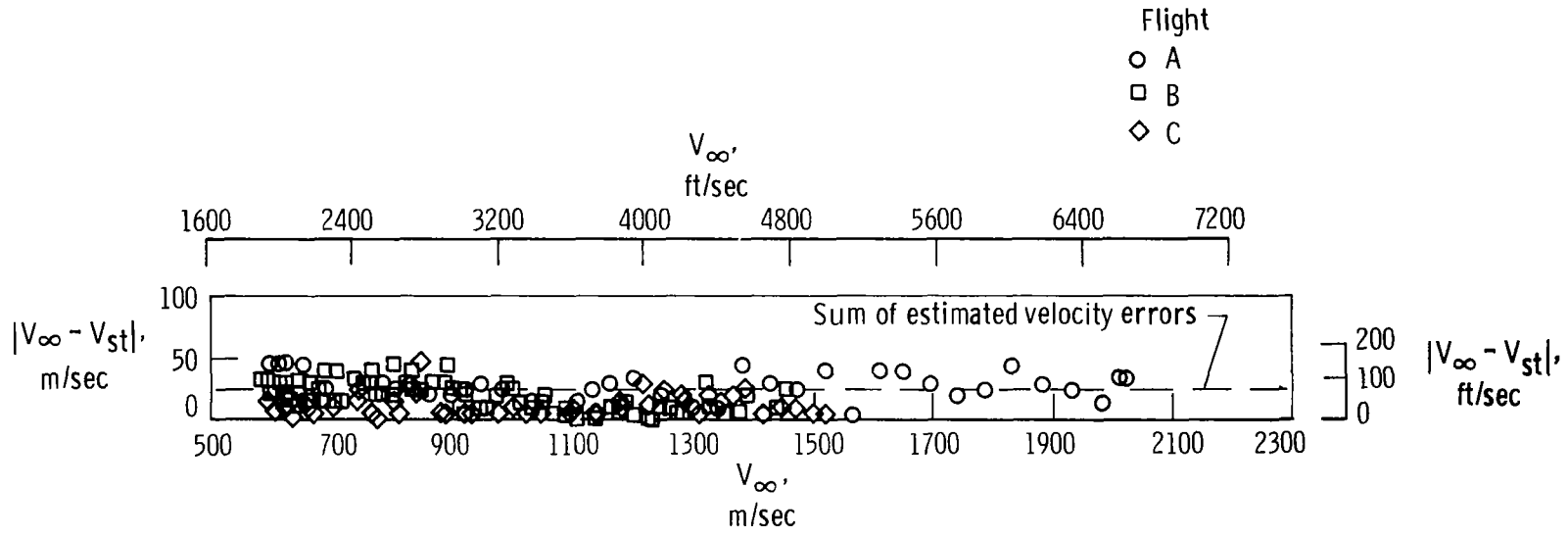

Figure 21. Absolute values of the velocity difference between V_∞ and V_{st} for a range of V_∞.

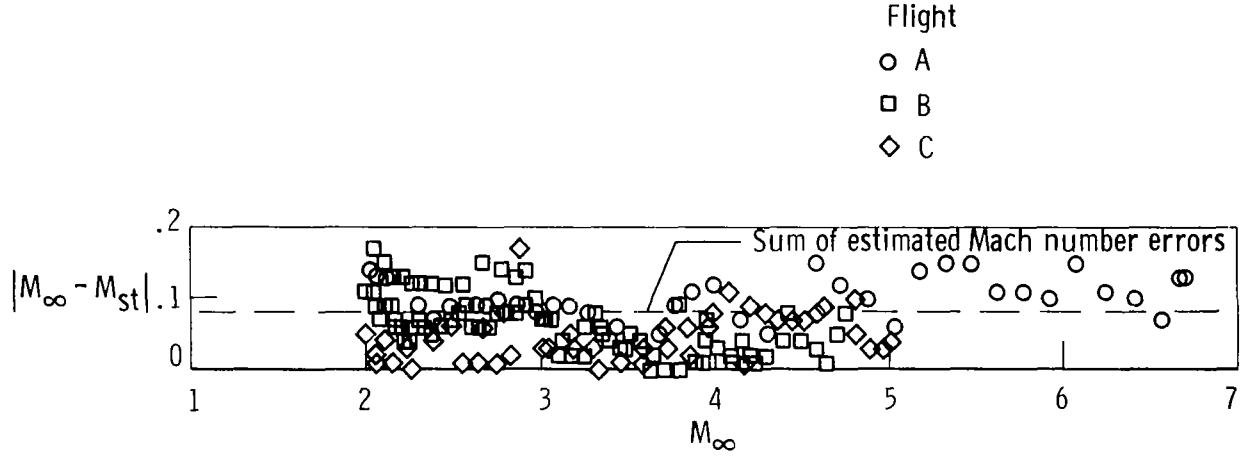

Figure 22. Absolute values of the Mach number difference between M_∞ and M_{st} for a range of M_∞.

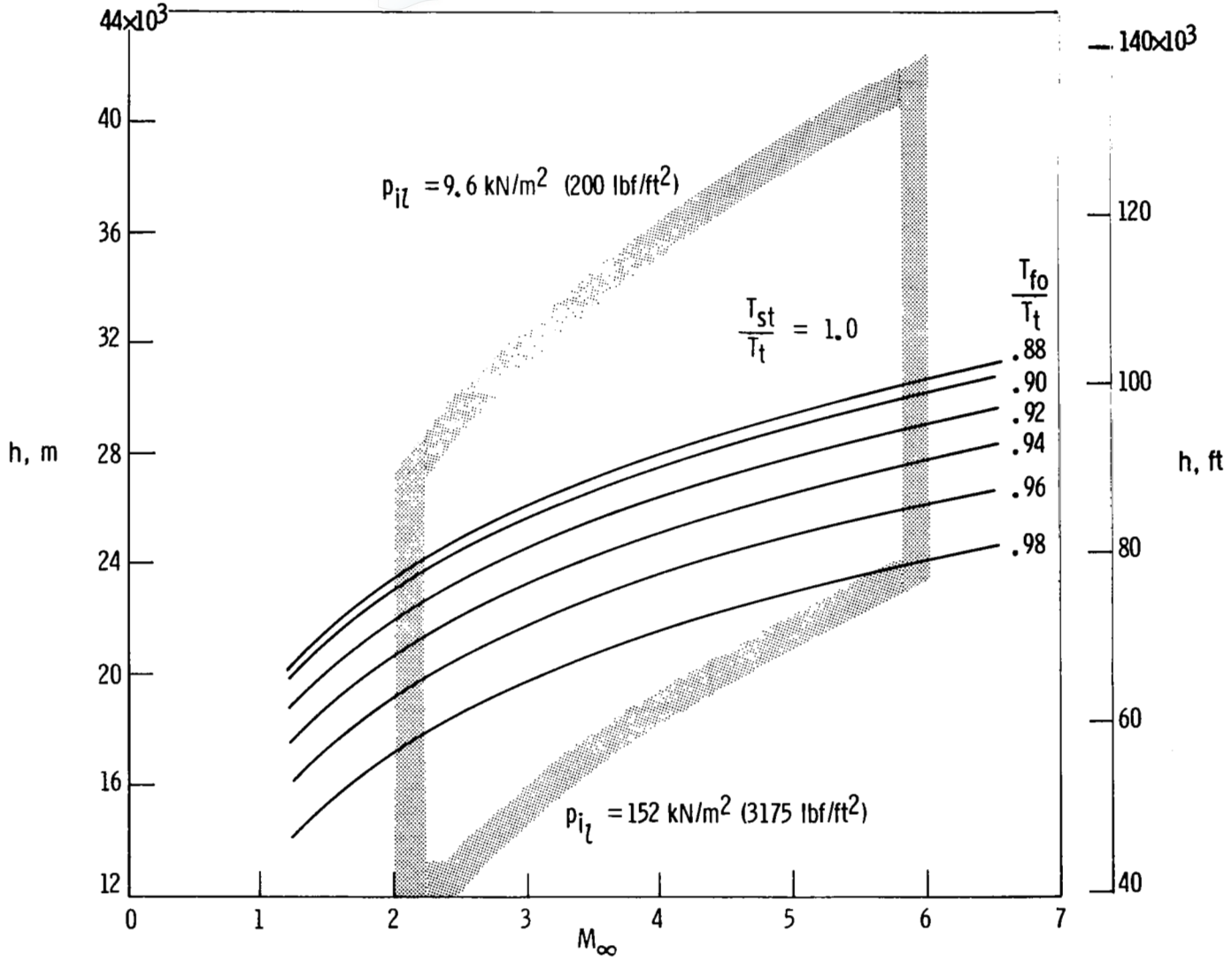

(a) Temperature correction factor.

Figure 23. Comparison of air-data correction factors for both probes plotted on a Mach number-altitude background.

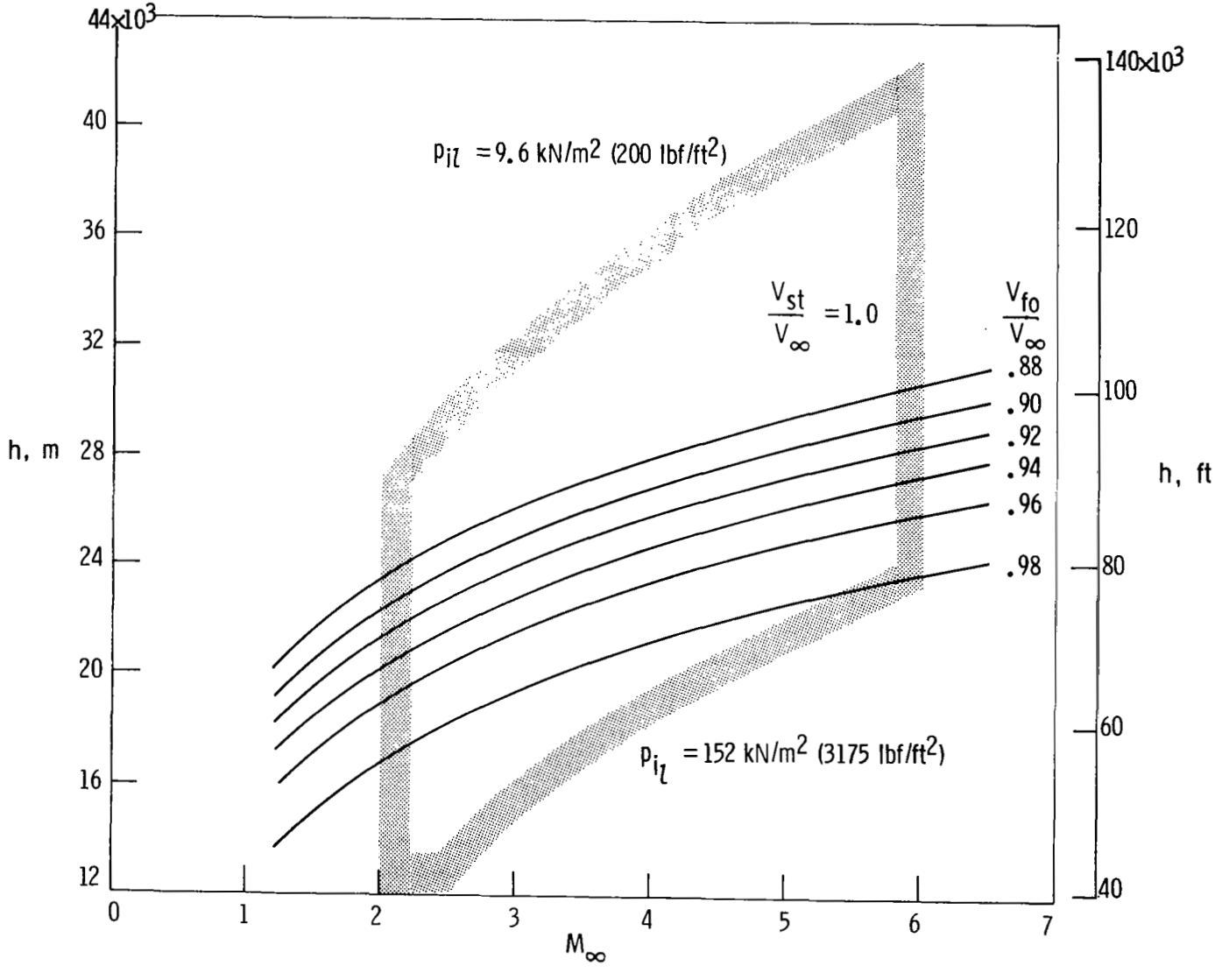

(b). Velocity correction factor.

Figure 23. Continued.

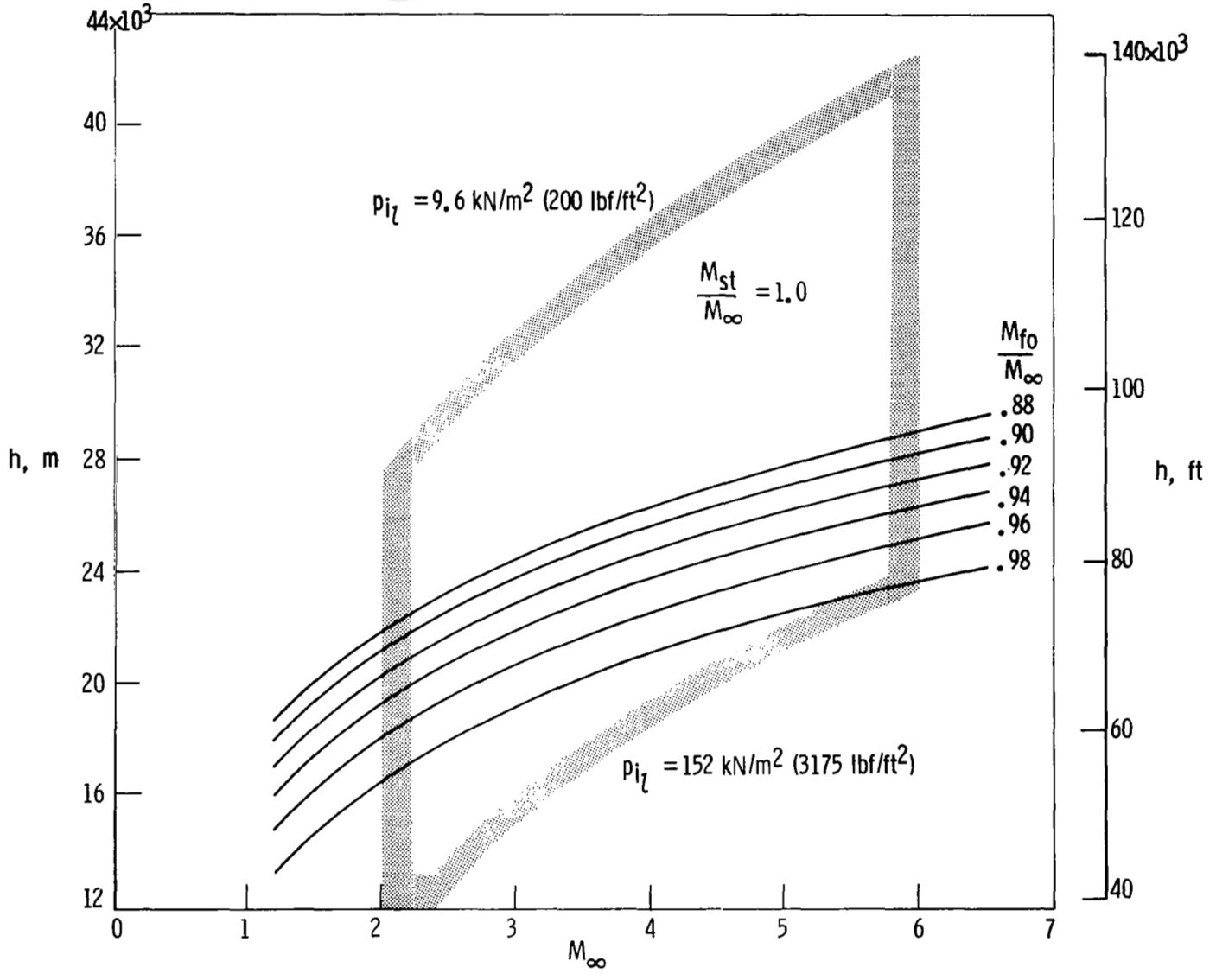

(c) Mach number correction factor.

Figure 23. Concluded.